FFI-RAPPORT

20/02334

Thermal stability of NMC442 cathode material studied by accelerating rate calorimetry

Susanne Hansen Troøyen
Torleif Lian

Thermal stability of NMC442 cathode material studied by accelerating rate calorimetry

Susanne Hansen Troøyen
Torleif Lian

Norwegian Defence Research Establishment (FFI) 7 December 2020

Keywords
Li-ionbatterier
Sikkerhet
Termisk materialprøving

FFI report
20/02334

Project number
1479

Electronic ISBN
978-82-464-3289-2

Approvers

Arvid Melkevik, *Research Manager*
Håkon Storli Andersen, *Director of Research*

The document is electronically approved and therefore has no handwritten signature.

Summary

Lithium ion batteries have developed into one of the most popular secondary batteries on the market today due to high voltage, long lifetime and high energy density. However, lithium ion batteries may have safety issues, and several fires are reported. Thermal stability is one of many parameters used to evaluate the safety aspects of lithium ion batteries. Understanding thermal stability at material level is essential for the further development into safer lithium ion batteries.

The thermal stability of $LiNi_{0.40}Mn_{0.37}Co_{0.23}O_2$ cathode material from a Kokam 8 Ah pouch cell with 1 M $LiPF_6$ in EC/DMC (1:1) was studied by accelerating rate calorimetry (ARC). Currently, there are no standard procedures for ARC tests on battery materials, and it is unknown how changes in the ARC setup would affect the outcome of the tests. Four different calorimetry test setups were tested in order to understand the influences of the setup on the result: A side plug setup (where the sample was placed in a sealed tube attached to the calorimeter lid), a side branch setup (where the sample in the lid was connected to an external gas system), a high-volume setup (with a 500 mL volume expansion of the gas system) and a throne setup (where the sample was placed in an insulated throne on the calorimeter floor). Regardless of the setup, the cathode/electrolyte mixture was found to have two stages of self-heating, where the rate of the first stage influenced the temperature at which thermal runaway (heating rate > 10°C min^{-1}) occurred during the second stage. It was proposed that a drop in temperature rate between the two stages of heating could be due to endothermic processes. During the initial stage of self-heating (175–240°C), the setup was not found to impact the results, and variations at this stage was attributed to personal errors in the sample preparation procedure. At temperatures above 240°C, the reactivity was found to be highly dependent on pressure. Samples at low pressure (near 1 bar) did not reach thermal runaway, whereas the samples in the higher-pressure setups all reached thermal runaway at 250–260°C. Thus, it was concluded that the test setup is very important for the outcome of the test, and the reactivity of the cathode material is dependent on pressure. The onset temperature for exothermic activity was consistently 175±5°C for all the material tests. Higher thermal reactivity was measured for the full cell, which had an onset temperature of 92°C and reached thermal runaway at 210°C.

Sammendrag

Litium-ion batterier har utviklet seg til å bli en av de mest populære batteriteknologiene i dagens marked. Dette kommer hovedsakelig av høy energitetthet, lang levetid og høy spenning. Men det har blitt rapportert flere branner knyttet til litium-ion batterier, noe som viser at sikkerhetsegenskapene til denne teknologien kan være en utfordring. Ved vurdering av sikkerheten til litium-ion batterier er termisk stabilitet en av flere viktige egenskaper som bør evalueres. Forståelse av termisk stabilitet på materialnivå er essensielt for videre forbedring av sikkerhetsegenskapene til litium-ion batterier.

Den termiske stabiliteten til katodematerialet $LiNi_{0.40}Mn_{0.37}Co_{0.23}O_2$ fra en Kokam 8 Ah litium-ion posecelle med 1 M $LiPF_6$ in EC/DMC (1:1) ble undersøkt med ARC (accelerating rate calorimetry). Metoder for måling av termisk stabilitet er ikke standardiserte, og det er usikkert hvordan endringer i ARC-testoppsatsen vil kunne påvirke resultatene. Fire ulike testoppsatser ble derfor testet: én med prøven festet i lokket av kalorimeteret, to hvor det ble koblet på et trykksystem (stort og lite volum) og én hvor prøven ble satt i en trone som var termisk isolert fra kalorimeteret. For alle oppsatsene ble det observert to selvoppvarmingsfaser. Det ble observert at selvoppvarmingsraten gjennom den første fasen påvirket ved hvilken temperatur ukontrollert temperaturutvikling (oppvarmingsrate > 10°C min^{-1}) startet i den andre fasen. En nedgang i oppvarmingsrate ble observert mellom de to fasene, og det ble foreslått at endoterme prosesser var årsaken til nedgangen. I den første fasen hadde oppsatsen ingen signifikant påvirkning på testresultatet, men selvoppvarmingshastigheten ble påvirket av variasjon i prøvepreparereingen. Ved temperaturer over 240°C kunne man se at reaktiviteten var avhengig av trykket, som igjen påvirkes av oppsatsen. Ved lavt trykk ble ikke ukontrollert temperaturutvikling oppnådd, mens det for testene med høyere trykk oppsto en ukontrollert temperaturutvikling ved 250–260°C. Resultatene viser at termisk stabilitet til det testede katodematerialet er trykkavhengig og at oppsatsen kan påvirke resultatene. For en hel litium-ion celle (Kokam 8 Ah) var starttemperaturen for selvoppvarming 92°C, og ukontrollert temperaturutvikling skjedde ved 210°C.

Contents

1 Introduction

Lithium ion batteries (LIBs) are currently the most popular secondary batteries on the market, being used in areas ranging from portable electronics to electronic/hybrid vehicles (1). The increasing demand for high-energy, lightweight rechargeable batteries has led to growing interest in research on safety and materials for LIBs since their commercialization by Sony in 1991 (2, 3). As the capacity of the batteries increases, the consequences of failure become more severe because there is more energy to be released in the case of short circuit. The thermal stability of LIBs is affected by several factors, including the composition of the electrolyte solution, the cathode and anode materials, as well as age and storage of the cell (4). Thus, the information obtained from thermal stability studies of complete cells is more understandable when paired with information about the separate materials.

The present study is aimed towards understanding how the setup of thermal stability tests of LIB cathode materials by accelerating rate calorimetry (ARC) can influence their results. This is investigated because there are currently no standard procedures for how to carry out ARC tests on LIB materials, and most authors mention little about sample preparation, sample containers and ARC setup. Understanding how the setup and sample preparation may affect results will make it easier to compare results from literature, and explain the events observed in the ARC tests. The goal is to develop a reproducible sample preparation procedure and gain knowledge about the effects of test setup. Additionally, a thorough study of cathode/electrolyte reactivity will be executed. This is an important part of the setup analysis, because understanding the specific processes will lead to awareness of how factors like pressure and heat transport is connected to the reactivity of the sample. The cathode material test results will be compared to the results of a full LIB cell in order to better understand the role of the cathode in LIB thermal stability.

1.1 Lithium ion batteries

A LIB consists of electrochemical cells (figure 1.1) where lithium ions are transferred between the anode and the cathode as the battery is charged and discharged. The flow of lithium ions inside the cell is accompanied by electrons flowing through an outer circuit, generating a current that can be used to power electronic devices (5). The negative electrode, or anode, is typically made up of graphite deposited on a copper current collector. Several materials can be used as the positive electrode, or cathode, which usually is coated onto an aluminium current collector (6). Since the introduction of lithium metal oxides (like $LiCoO_2$) as promising cathode materials, nickel-rich lithium metal oxides like $Li(Ni_xMn_yCo_z)O_2$ (NMC) are now some of the most popular cathode materials for high-capacity LIBs (1, 7-9).

Physically separating the two electrodes is normally a polyethylene and/or polypropylene (PE/PP) separator that is electrically insulating, but permeable to lithium ions (10). Lithium hexafluorophosphate ($LiPF_6$) dissolved in a mixture of organic carbonate solvents, like ethylene

carbonate (EC), ethyl methyl carbonate (EMC), dimethyl carbonate (DMC) and diethyl carbonate (DEC), is the most common LIB electrolyte (5, 11, 12).

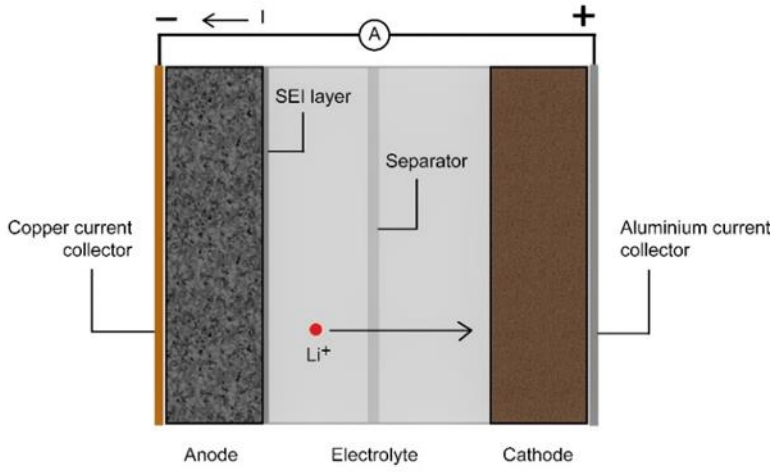

Figure 1.1 A lithium ion cell during discharge.

The operating voltage of LIBs exceeds the electrochemical stability window of the electrolyte, which leads to formation of a solid electrolyte interphase (SEI) at the anode surface due to reduction of the electrolyte solvents by the anode, as described by Goodenough *et al*. (13). This layer starts to form during the first cycle of charging, and it is essential for proper operation of the battery as it protects the electrolyte from being further reduced (14). The formation of the SEI layer consumes lithium ions, which could lead to capacity loss.

Much of the research on LIBs aims to increase the energy density of the batteries, whilst keeping them stable and safe to operate (2, 15). However, increased energy density poses serious safety issues for LIBs as higher energy density is associated with lower thermal stability (8).

1.2 Safety of lithium ion batteries

Despite all the research being done on LIBs, there is still a long way to go before the high energy and safety demands will be met. Even with the batteries on the market today there is a possibility of overheating, which in a LIB could result in fire and/or explosions. Some dramatic incidents have been reported with electric vehicles, which underline the importance of attention to battery safety (16, 17).

One of the main safety issues in LIBs is the electrolyte, which is volatile and highly flammable and may release substantial amounts of gas and heat if the temperature reaches a certain point (3, 18). Stabilizing and flame-retardant additives are common, but they only work to a certain extent and may limit the performance of the cell (18, 19). Overheating in a battery is usually initiated by factors such as overcharge, exposure to high temperatures and internal or external

short circuits (17, 20). Thermal processes inside the cell can induce further self-heating which eventually may lead to thermal runaway – a self-enhancing exothermic process that may cause fire and/or explosions. Normally, thermal runaway is defined as a self-heating rate exceeding 10°C min^{-1} (20).

To increase the safety of LIBs, one has to look beyond the cell itself and evaluate the safety of the battery pack, module and how the battery is integrated in electric vehicles. The battery management system (BMS) is an important safety feature of LIB packs. Its functions include monitoring and control of temperature, voltage and current (20-22).

In the same way that safety should be evaluated beyond the cell level, it should also be considered on a material level, and the thermal stability of individual components of a LIB cell should be studied. This way it will be easier to point out, and thus work towards preventing, specific sources of self-heating in the full battery.

1.3 Testing thermal stability of battery materials

1.3.1 Instrumental methods

Calorimetric methods are widely used in thermal stability tests for LIB components. Accelerating rate calorimetry is one of the most popular methods used to analyse individual components and full cells. It is based on recording the self-heating of a sample in a semi-adiabatic environment (23, 24). This is achieved through a heat-wait-seek procedure, where the sample is heated to a set temperature, then waits for a period of time to establish equilibrium. After the wait period, the system enters seek mode where it searches for exothermic activity with a sensitivity of 0.02°C min-1 (20). If exothermic reactions are not detected, the cycle is repeated until they are. The system then enters exotherm mode, where the self-heating of the sample is tracked under adiabatic conditions. The calorimeter follows the heating of the sample so that no heat is lost to the environment.

Differential scanning calorimetry (DSC) is another popular method for testing thermal stability of materials. It is less sensitive than the ARC, and uses smaller sample sizes (20, 25). DSC experiments are based on measuring the difference in heat flow from a pan containing the sample and an empty reference pan, whilst heating them both at a predetermined rate (26). If endothermic or exothermic reactions occur in the sample, it will be registered by the difference from the reference pan.

In addition to calorimetry, it is often interesting to determine the weight loss of a material as it is heated. Thermal gravimetric analysis (TGA) is a method for accurately weighing a small amount of material during heating, in order to obtain a plot of weight percent as a function of temperature (27). Weight loss during heating may be due to several factors such as decomposition, phase transitions with gas release, and evaporation of solvents (28). TGA is sometimes combined with DSC or differential thermal analysis (DTA), which makes it possible

to see the thermal characteristics (endothermic and exothermic reactivity) of a sample together with the gravimetric changes.

To get additional information about material structure and morphology, ARC or DSC experiments are frequently supported by scanning electron microscopy (SEM), X-ray diffraction (XRD), energy dispersive spectroscopy (EDS) and inductively coupled plasma mass spectroscopy (ICP-MS) to study surface structure, crystal structure and elemental composition of materials (29). Analysis of gas products from decomposition of battery materials can be performed by gas chromatography/mass spectroscopy (GS-MS).

1.3.2 Comparing methods and reproducibility

All of the previously mentioned instrumental methods give insight into different aspects of thermal stability of LIB materials. It is very important to be aware of their differences. Since they measure different properties based on different principles, it can be hard to compare output between methods. As an example, the high ARC sensitivity (0.02°C min^{-1}) makes it able to record weak exotherms that the DSC cannot detect with a heat ramp of 5-10°C min^{-1} (25, 30-32). The heat rate and sample size of a DSC experiment may influence the recorded onset temperature and total heat of an exothermic reaction (25, 33).

Not only is it problematic to compare results from different instrumental methods, there can also be large variations between measurements from the same method. Factors such as sample size, sample holder, preparation technique, pressure, etc. may influence the results of ARC experiments (34). Additionally, the electrode: electrolyte ratio has been found to influence the recorded exothermic activity in ARC experiments (35).

Shurtz *et al*. have stressed the importance of describing sample holder in detail, but few reports actually do this (34). The sample holder in an ARC experiment will absorb heat generated by the sample, which means that the recorded temperature rise will be lower than the actual heat released by the sample. The heat lost by the sample container can be explained by the φ-factor,

$$\varphi = 1 + \frac{m_b c_b}{m_s c_s} \quad (1)$$

where m is the mass, c is the specific heat capacity, and the subscripts b and s are the bomb and sample, respectively (24). If other heat absorbing elements are present, they too should be added in the numerator. Although rarely mentioned in literature (36, 37), the φ-factor is very useful for evaluating how well ARC tests correspond to a real situation. Ideally, the φ-factor of an experiment should be close to that of the full lithium ion cell.

1.3.3 Existing research on NMC cathode materials

Several studies on the thermal stability of LIB components have been published. Dahn's group have conducted many ARC experiments on NMC442 (35, 38, 39) and other NMC cathode materials (39-44). Hildebrand *et al*. have also reported ARC results on NMC442 (37). None of the published results on NMC442 are based on the 1 M $LiPF_6$ in EC/DMC electrolyte solution

which is used in the present study. The work of Röder *et al*. on ARC studies of an NMC/LCO blend and electrolyte solutions is also valuable when evaluating the thermal stability of NMC442 (32, 36, 45). The existing ARC results for NMC442 normally have somewhat different values for onset temperatures and heating rates during the exothermic activity. The onset of a sustained exothermic reaction lies around 150-190°C, and thermal runaway is reached at 265-285°C (35, 37-39). It is not possible to describe the exact cause of the differences based on these few studies alone. However, different electrolyte composition, material preparation, Ni, Co and Mn content and ARC setup may be possible causes. This is why research on the ARC setup is important; it may explain some of the variance observed in literature.

It is crucial to look further than ARC studies only, to gain perspective on the subject from different angles. DSC measurements on NMC materials usually have higher onset temperatures, which could be due to lower sensitivity. The DSC and TGA results found in literature are especially useful for identifying endothermic activity and O_2 release in samples (30, 31, 46-48). The work of Bak *et al*. on XRD measurements of different grades of NMC gives a comprehensive overview on the thermally induced phase transformations of NMC based on composition (49). They showed that NMC433 is only slightly more thermally stable than NMC532, whereas a big reduction in thermal stability is seen with NMC622. From this, it can be assumed that NMC442 could be compared to NMC materials in the composition range between NMC433 and NMC532.

1.4 Chemical reactions and processes inside a lithium ion battery

1.4.1 $LiPF_6$ electrolyte solutions

To get a grasp on the reactions occurring inside the LIB as it is heated, it is convenient to first have a look at the reactions that may happen during thermal decomposition of separate components. Due to its central role in thermal decomposition, the electrolyte is a good place to start. The thermal reactivity of $LiPF_6$ in carbonate solvents is complex, but thoroughly studied in existing literature (50-59). It is well known that the $LiPF_6$ salt will decompose to LiF and PF_5, both as a solid and in solution, following reaction I (53, 55). The species exist in equilibrium, which means that the decomposition depends on pressure.

$$LiPF_6\,(s) \rightleftharpoons LiF\,(s) + PF_5\,(g) \qquad \text{(I)}$$

It is known that the strong Lewis acid PF_5 will react further with the carbonate solvents, with similar mechanisms and decomposition products for every solvent, but different reactivity (50, 52, 58). Kawamura *et al*. and Gnanaraj *et al*. explained that endothermic monomolecular elimination of ethylene from DEC occurs when PF_5 attacks the lone pair of the carbonyl oxygen (58, 59). This is not observed for EC and DMC because they do not contain ethylene, which could explain that $LiPF_6$ solutions with DEC have been shown to have lower thermal stability than those with DMC (52, 59). The linear carbonates may also undergo PF_5 catalysed elimination with carbocation intermediates, which is also favoured for DEC as it will give a more stable intermediate. A similar PF_5 attack on EC has been shown to induce endothermic ring opening of

EC, which further causes a polymerization reaction that releases CO_2 (50, 52, 54). At higher temperatures, transesterification reactions of DEC and DMC leads to formation of EMC (53, 58). In the same way that PF_5 reacts with carbonyl lone pairs, it will also attack trace water and alcohols in the electrolyte solution, following equation II (53, 56-58).

$$PF_5 + H_2O \rightarrow PF_3O + 2HF \qquad \text{(II)}$$

The highly reactive products from this reaction catalyses further decomposition. Breakdown of the electrolyte may release toxic gases such as CO and HF (52, 60).

1.4.2 NMC cathode materials

Although there are many types of cathode materials, only reactions involving NMC (or $LiMO_2$, M = Ni, Mn, Co) will be discussed here. For the NMC materials, high Ni content is associated with lower stability and higher capacity (1, 8, 39, 49). It is well known that thermal degradation of NMC is accompanied by O_2 release (49, 61-63). This is due to the thermally induced phase transitions layered NMC → Mn_2O_4 spinel → Mn_3O_4 spinel → rock salt, as explained by Bak *et al*. (49).

These phase transitions are inevitable at elevated temperatures, but the temperatures at which they occur is highly dependent on the amount of Ni, Mn and Co in the material (40, 49). Several studies have concluded that increasing the relative amount of Ni will lead to lower onset temperatures for phase transitions and increased amount of O_2 and heat generated (39, 40, 49). Higher state-of-charge (SoC) will also lead to higher reactivity for NMC (25, 37, 39).

Decomposition of the electrolyte is affected by the supply of O_2 from the cathode, as it may oxidize the solvents, as shown in equations IIV and IV (11, 32, 37, 62, 64).

$$C_3H_4O_3 \text{ (EC)} + 5/2\ O_2 \rightarrow 3\ CO_2 + 2\ H_2O \qquad \text{(IIV)}$$

$$C_3H_6O_3 \text{ (DMC)} + 3\ O_2 \rightarrow 3\ CO_2 + 3\ H_2O \qquad \text{(IV)}$$

Röder *et al*. showed, by using very small amounts of EC/DMC together with an NMC/LMO blend, that the oxygen release will catalyse solvent breakdown (32). They found that self-heating of the solvent was directly correlated to the self-heating of the pure cathode material associated with O_2 release.

The thermal decomposition of the electrolyte versus the cathode, and the mixture of the two, is complicated. MacNeil and Dahn discovered that the addition of EC/DEC solvents to $LiCoO_2$, increased the reactivity, lowering the temperature for a heat rate above 1°C/min by about 140°C (61). This is because of the reactivity of the solvents. Another interesting observation from the same study is that addition of $LiPF_6$ to the solvent/cathode mixture was shown to inhibit the reaction between them. They attributed this to polymerisation products depositing on the cathode surface hindering oxygen release which slows down decomposition of the electrolyte solvents (65). Later reports by Wang *et al*. showed that this effect only applied to $LiCoO_2$, - the

opposite was observed for NMC (35). For NMC, the reactivity usually increases with increasing electrolyte content. These results are interesting because they illustrate how much the different compounds influence the stability of each other. The amount of electrolyte solution versus cathode material also has an influence on the reactivity (32, 35).

1.4.3 Complete cells

The reactions of the full cell are more complex, because reactions between the components of the cell are introduced. It is not as useful to know the specific reactions, as it is to know which components are involved in the different stages of heating. In this text, the focus lies on the cathode, but the anode also generates heat at a certain temperature (23, 25, 46, 66, 67). Generally, the anode is associated with the earliest self-heating in a battery, where the SEI layer breaks down and intercalated lithium reacts with the electrolyte to form a new metastable SEI layer (30, 68). If the temperature increases further, electrolyte and cathode decomposition occur, and the separator melts (3). This may create short-circuits in the cell and heat release. Liu *et al*. showed that thermal runaway of LIBs is not exclusively due to short-circuiting, but it can be initiated by chemical crossover reactions between the anode and cathode, where released O_2 from the cathode reacts with the anode (30).

1.5 Objectives

The lack of standardised methods for ARC measurements has been a major motivation for the current study. Understanding the influence of the ARC setup on the results of each test will be valuable in future work, and it will help to more critically evaluate existing literature. Four different ARC setups will be tested for the same cathode/electrolyte sample. The first is a simple, pressure tight setup, where the sealed sample is connected to the ARC lid. Next, pressure measurements will be introduced, which requires connection of the sample to an external gas system. This will be done through a side branch with a Swagelok quick connector, which facilitates easy transport of the sample from the glove box without a chance of air contamination. As the influence of pressure on cathode thermal reactivity has not been studied systematically before, another setup where the volume of the gas system has been expanded by 500 mL will be tested as well. A reference setup without lid connection will also be tested by placing the sample in a thermally insulated throne on the calorimeter floor. This setup is not pressure tight, and could perhaps resemble reality (where venting would occur at a certain pressure) more than the sealed tubes. Lastly, the cathode material tests will be compared to a full lithium ion cell test, for a more comprehensive evaluation of thermal stability. The ARC measurements will be complemented with TGA and SEM/EDS analysis.

2 Experimental

2.1 ARC preparations

ARC material tests were performed on a Thermal Hazard Technology esARC accelerating rate calorimeter (figure 2.1), which was prepared with calibration and drift tests before every change of setup, and regularly throughout the testing period. The drying/calibration/drift test procedure is described in the THT esARC manual (24).

Figure 2.1 The esARC.

A standard sample test was performed with 20% di-tert butyl peroxide (DTBP) in toluene in a Ti bomb (see figure 2.2), which was compared with literature (69).

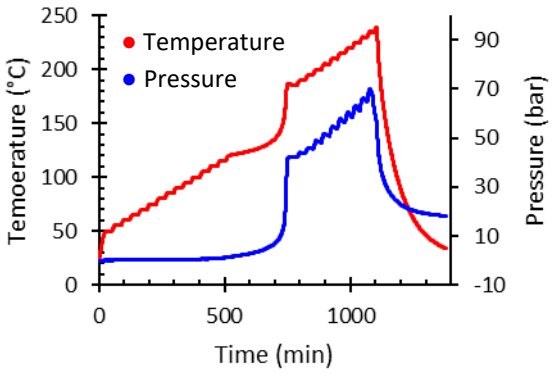

Figure 2.2 Temperature and pressure as a function of time for 20% DTBP in toluene.

Pressure measurements were implemented via an external gas system (figure 2.3), which also allows for gas sampling from the ARC tests. For the DTBP and electrolyte test, a 3000 psig

(207.9 bar) pressure transducer was used. For all the other tests, a 200 psig (14.8 bar) pressure transducer was used. The external fixture has a total volume of 38 mL (not including the gas sample bottle or side branch/sample tube). The volume was estimated by assuming ideal gas expansion from a known volume (gas sample bottle of 50 mL) to the unknown volume of the whole external fixture. This was done by first filling the entire system with Ar, and measuring p_1. Then, the sample bottle valve was closed. The rest of the fixture was evacuated and p_2 was measured after opening the sample bottle again.

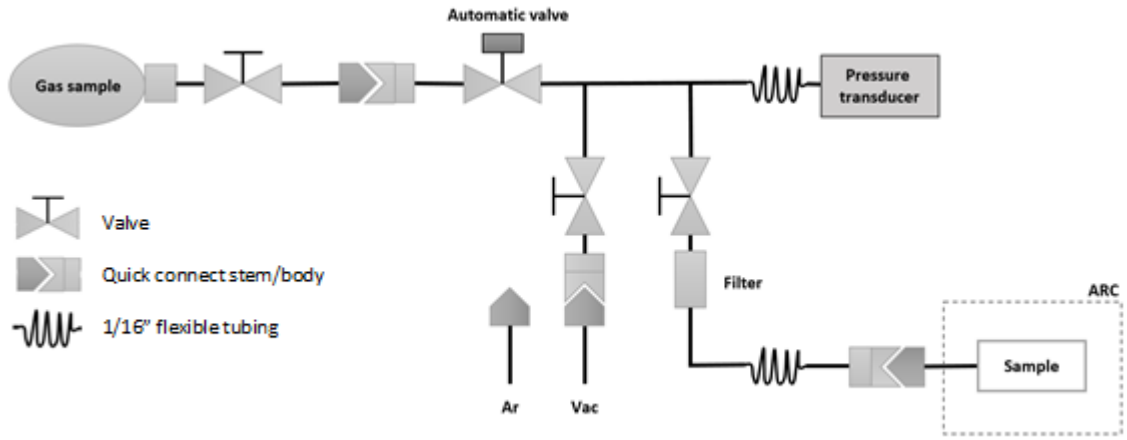

Figure 2.3 Schematic representation of the pressure tight gas system.

2.2 Material preparation

All material tests were performed with delithiated NMC442 ($LiNi_{0.40}Mn_{0.37}Co_{0.23}O_2$) from a Kokam 8Ah pouch cell at 100% SoC. SEM images and EDS analysis for an identical cell is shown in appendix A. The cell was cycled according to the following regime; constant current (CC) (1.6 A) discharge to 3.0 V, 60 min break, CC (1.6 A) charge to 4.2 V, constant voltage (CV) charge to <0.4 A, 60 min break, a total of four times. Opening of the cell was performed inside an Ar-filled MBRAUN glove box with O_2 and H_2O levels <0.1 ppm and a nitrogen purifier.

After opening, the cathode sheets were kept in a sealed Al pouch inside the glove box. When ready for an experiment, the electrode was taken out of the pouch and washed two times with pure DMC for 2 min, as recommended by Waldmann *et al*. (29). After washing, the cathode material was scraped off the current collector with a scalpel. This was done while the material was still wet, as it made it easier to scrape it off. The powder was then dried for 1 hr under vacuum in the glove box antechamber, before it was left overnight in the glove box. After this, it was stored in a closed container inside the glove box. The material from one cathode sheet was sufficient for 2-3 ARC tests.

2.3 ARC experiments

2.3.1 1 M $LiPF_6$ in EC/DMC (1:1)

The electrolyte solution used for all tests was 1 M $LiPF_6$ in EC/DMC (1:1), obtained from Sigma Aldrich (product no. 746711). It is hereby often referred to as the electrolyte solution. For a separate electrolyte test the electrolyte solution (500 µL) was placed in a Ti bomb (ARCTC-Ti-HBQ, 0.8 mm wall thickness) in the glove box. A lid was placed over the opening of the bomb before it was removed from the glove box. It was attached to the side branch in the calorimeter lid with a Swagelok fitting while flushing the side branch with Ar to prevent air exposure. The thermocouple was placed at the bottom of the bomb, as shown in figure 2.4. The ARC test was run from 50-405°C, with temperature steps of 5°, a 15 min wait time and a sensitivity for exothermic activity of 0.02°C min^{-1}.

Figure 2.4 Setup for the electrolyte ARC test.

2.3.2 NMC442 with 1 M $LiPF_6$ in EC/DMC (1:1)

For all the cathode material tests, stainless steel (SS) tubes (ARC-ES-1750, ~1.32 g, 5.5 cm length, 0.15 mm wall thickness, welded on one side, heat capacity c_{SS} = 0.50 J K^{-1} (70)) were used as sample containers. Before the tests, they were washed with HNO_3 (conc.) for 30 min and pure water for 2x10 min, then rinsed with acetone and dried.

The dried NMC442 cathode powder (0.600 g) was transferred to the tube using a weighing funnel with an attached pipette tip (figure 2.5). The electrolyte solution (0.30 g, 231 µL) was then added. A small amount (~15 mg) of ceramic insulation material was placed above the sample in the tube to keep the material in place. The tube was sealed with a Swagelok nut to the appropriate fixture before removing it from the glove box to be placed in the calorimeter. Due to the thin walls of the tube, the nut was screwed only one full round (it would normally be 1 ¼) after tightening it by hand. This setup was confirmed to be pressure tight by testing under high pressure before the ARC tests. This was done by connecting to a side branch, filling with approximately 5 bar Ar, and waiting to verify that the pressure did not decrease over time.

Figure 2.5 Weighing funnel used to transfer the NMC material to the tube.

The sample thermocouple was placed 2.2 cm above the bottom of the tube with an Al clip (c_{Al} = 0.91 J K^{-1} (71)) for all the setups. (Fiberglass tape was initially used to secure the thermocouple and isolate it from the Al clip, but it was later excluded because it seemed to influence the results. No fiberglass tape has been used in the results presented here). All of the ARC tests were run from 100-355°C, in 5°C increments, a wait time of 25 min and sensitivity for exothermic activity of 0.02°C min^{-1}.

Table 2.1 lists the ARC tests on the NMC442 cathode material with electrolyte, and refers to pictures of each setup. The first setup tested was a sealed SS tube attached to the calorimeter lid (side plug setup). The second was a sealed SS tube connected to the external gas system via a side branch for pressure measurements (side branch setup). The side branch was isolated with alumina tubes, preventing thermal contact between the branch and the calorimeter. This setup was also tested with increased volume, by attaching a 500 mL bottle to the external gas fixture (side branch with high volume setup). After every test using the side branch setup, the side branch was rinsed thoroughly with acetone and dried before the next test. A reference setup with the SS tube inside an isolated throne on the calorimeter floor was also run (throne setup). Here, the tube was pressed shut with pliers before removing it from the glove box. Three parallels of each setup were run, plus a fourth with the side plug setup that was run after all the other tests, to see if there had been any degradation of the material over time.

Table 2.1 List of cathode material ARC tests.

Setup number	Description	Parallel names	Figure
1	Side plug	1-1, 1-2, 1-3	2.6
2	Side branch	2-1, 2-2, 2-3	2.7
3	Side branch, high volume (+500 mL)	3-1, 3-2, 3-3	2.8
4	Throne	4-1, 4-2, 4-3	2.9

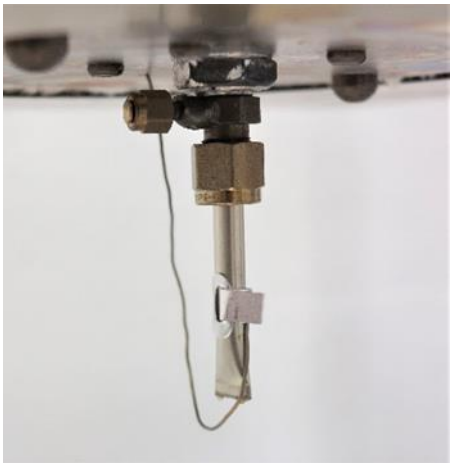

Figure 2.6 Side plug setup (1).

Figure 2.7 Side branch setup (2). The side branch was connected to the external gas fixture.

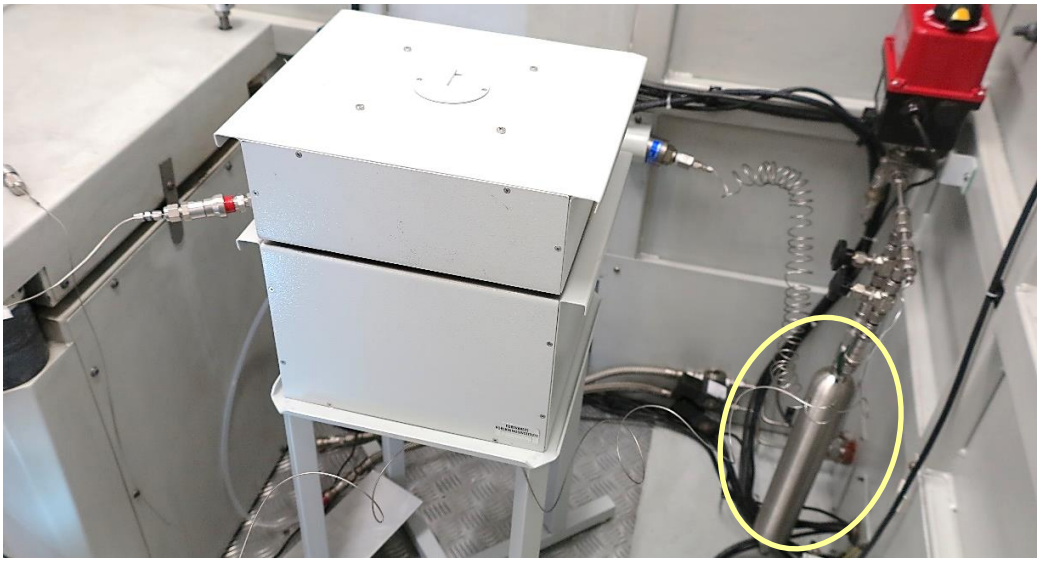

Figure 2.8 Side branch setup with 500 mL bottle connected to the external gas system (3).

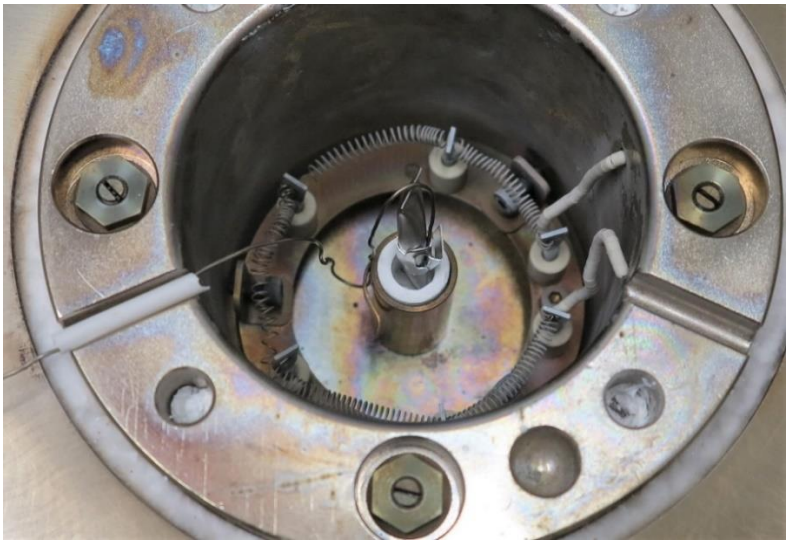

Figure 2.9 Throne setup (4).

2.3.3 Full Kokam 8Ah pouch cell

To measure the thermal stability of a 100% SoC full cell, a Thermal Hazard Technology EV+ accelerating rate calorimeter was used. Before testing the full cell, the calorimeter was calibrated and drift tested. The Kokam 8Ah cell was cycled as described in section 2.2, and placed in a lightweight Al fixture, isolated from the fixture with 10 mm Pyrogel XTE insulation from Aspen Aerogels. The thermocouple was placed on the center of the top of the cell. A 0.1 bar overpressure was applied to the cell by compressing four springs (spring constant k = 4.9 N/mm) at the corners of the fixture. Each spring was compressed 4.5 mm (5.5 rounds), which corresponds 0.1 bar applied pressure. The setup was then secured with four additional screws. Figure 2.10 shows the setup inside the EV+ ARC. The calorimeter was flushed through with Ar (0.1 bar) for 2 min, followed by a 2 min break a total of 4 times before the test. Then, the ARC was heated to 40°C before proceeding to the heat-wait-seek routine, with 5°C increments, 60 min wait time and 250°C end temperature.

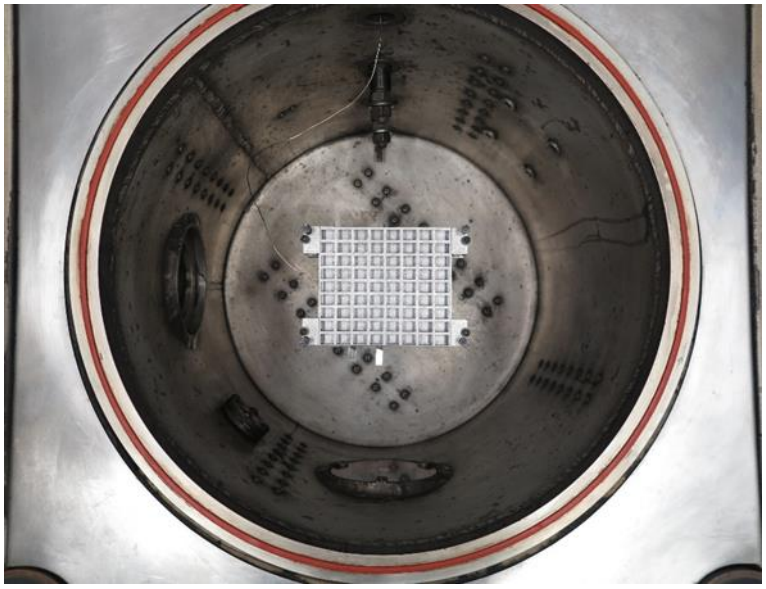

Figure 2.10 Full cell setup in the EV+ ARC.

2.4 TGA experiment

A TGA test (with DTA) was run with unwashed NMC442 material from an identical cell, on a TA instruments TGA5500. A Pt pan was tared on the instrument before adding the sample (16.58 mg) inside the glove box. The sample was transported directly to the instrument in a sealed container to limit air exposure. The experiment was run with a heating ramp of 5°C min^{-1}, an N_2 flow rate of 25 mL min^{-1} and a final temperature of 400°C.

3 Results

3.1 ARC experiments

3.1.1 1 M $LiPF_6$ in EC/DMC (1:1)

The electrolyte solution has an exothermic onset temperature of 215°C (see figure 3.1). The maximum heating rate is 0.92°C min^{-1}. The pressure increases slightly before the onset temperature, where it suddenly increases with about 30 bar during the exothermic process. The exothermic process is a collection of chemical reactions of the electrolyte solvents EC and DMC (explained in section 1.4.1) producing gases like CO_2, which leads to increased pressure.

Several studies have confirmed decomposition onset of electrolyte solutions at 180°C-215°C (36, 52, 58). Pressure increase before the exothermic onset is likely a combination of increased vapour pressure/evaporation of the solvent and slow endothermic decomposition of the $LiPF_6$ salt according to reaction I. There is also a smaller exothermic process detected at 341°C, with heating rate 0.04°C min^{-1}. After the test, there was no liquid left in the Ti bomb. It contained a grey powder, which could be solid LiF from reaction I.

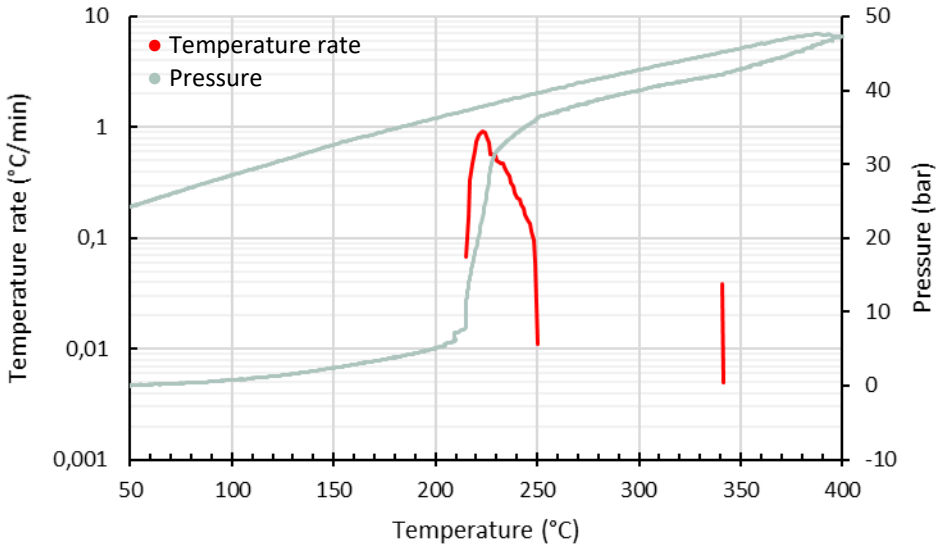

Figure 3.1 Self-heating rate and pressure for 1 M $LiPF_6$ in EC/DMC (1:1) as a function of temperature.

3.1.2 NMC442 with electrolyte – side plug setup

The self-heating curves of four equal ARC tests with the airtight side plug setup are shown in figure 3.2. Parallel 1-4 was measured 3 months after the others. Onset temperatures for exothermic behaviour are 170°C, 175°C and 180°C, giving an average of 174°C. As the ARC can only detect onset temperatures in 5°C increments, this deviation is to be expected. The exotherm starts with a slow rise in heating rate to a maximum of about 0.06°C min^{-1}, before the self-heating slows down without going below the detection limit. This can be described as the pre-thermal runaway phase of heat evolution. At 234°C (243°C for 1-4), there is a sharp rise in the heating rate that goes all the way to thermal runaway (>10°C min^{-1}). This can be thought of as the onset of thermal runaway, because of the quick acceleration to thermal runaway, which is reached at 250°C (262°C for 1-4).

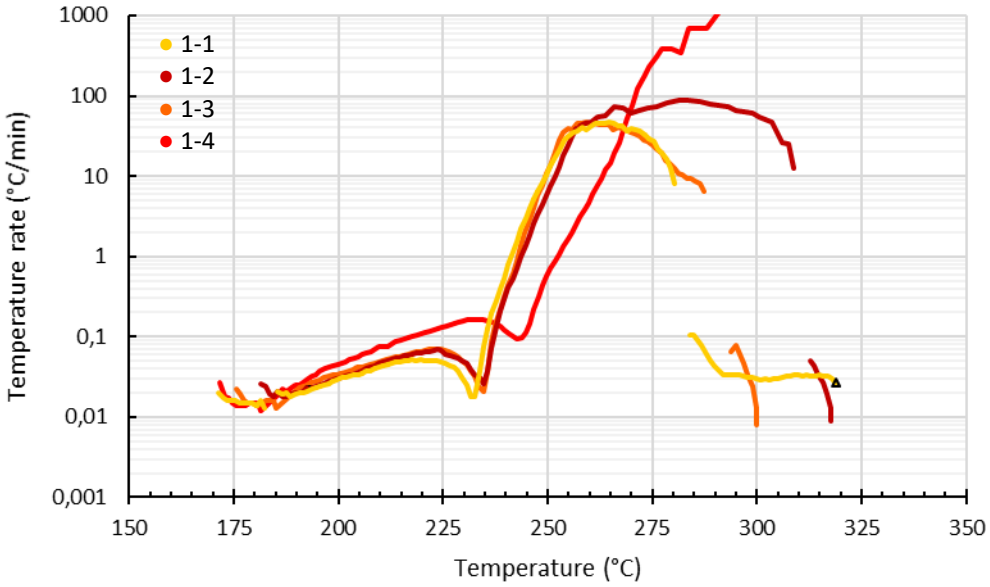

Figure 3.2 Self-heating of NMC442 with electrolyte solution in the side plug ARC setup.

The sudden stop of the self-heating curves after thermal runaway is due to negative heat rates recorded here. Negative heat rates cannot be displayed in a logarithmic plot. The cause of cooling of the sample will be discussed later. Test 1-4 did not experience the cooling effect, because it reached the end temperature of the ARC (355°C) during thermal runaway. Low exothermic activity is normally observed one or two heat-wait-seek cycles after the cooling. For test 1-1, the ARC test was interrupted at 319°C, which is marked with a triangle in the plot.

3.1.3 NMC442 with electrolyte – side branch setup

Figure 3.3 shows the ARC results from the side branch parallels, where pressure measurements were implemented. They also have very similar heat evolution. All parallels have an onset temperature for exothermic activity of 175°C. The temperature rate slowly builds to a heating rate of 0.16°C min^{-1}, which is almost three times higher than what was normally measured with the side plug setup. The heating then slows down before the onset of the thermal runaway process, which occurs at 242°C – that is, 8°C higher than for the side plug tests. At 260°C, the heating rate is at 10°C min^{-1}. Negative heating rate after thermal runaway was also recorded here. For test 2-1, the temperature drop was larger than the safety limit of the ARC experiment, which ended the experiment before any more exotherms could be detected.

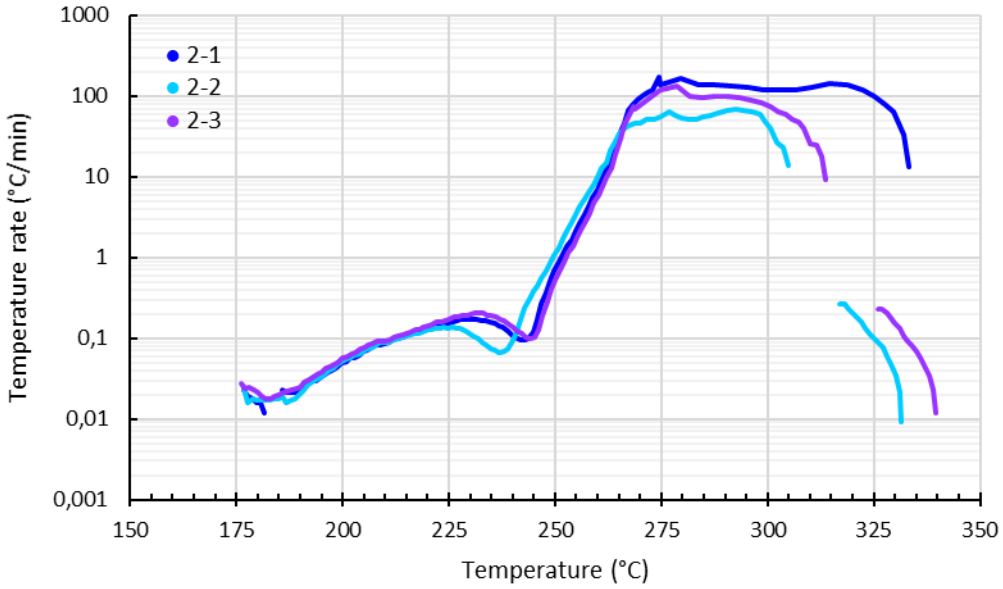

Figure 3.3 Self-heating of NMC442 with electrolyte in the side branch ARC setup.

Figure 3.4 shows the pressure measurements from tests 2-1, 2-2 and 2-3. There is a slight pressure rise starting around 100°C. At 175°C, where the exothermic onset is, the pressure increase is accelerated. There is no pressure drop where the negative heating rate is observed. Total pressure increase is around 4 bar.

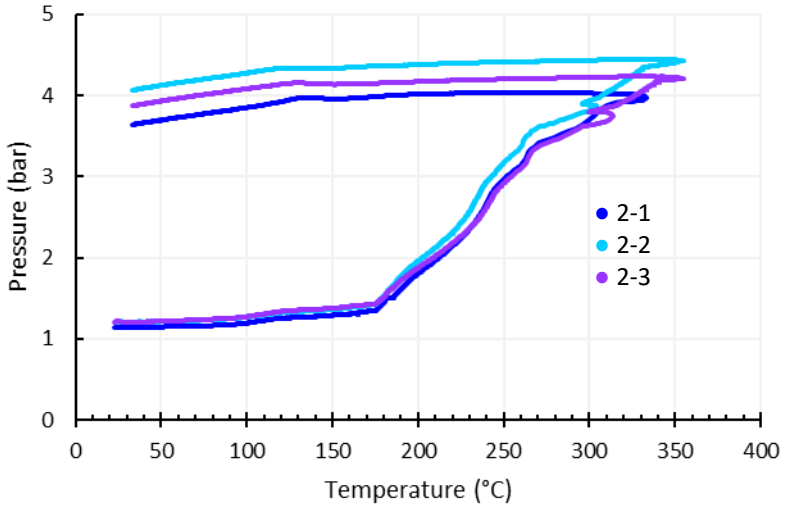

Figure 3.4 Pressure development through the side branch of the side branch tests.

3.1.4 NMC442 with electrolyte – side branch setup with 500 mL extra volume

Below are the self-heating curves recorded with the side branch setup with 500 mL of extra volume. Pressure measurements were implemented here as well. None of these tests reached thermal runaway, which shows that the thermal runaway reaction is dependent on the volume of the pressure system. The first stage of self-heating is initiated at around 175°C, with a slow rise to 0.09°C min^{-1}. After the heat rate has slowed down, the onset normally associated with thermal runaway is observed at 239°C. The maximum heating rate is 5°C min^{-1}, on average. After this, the heating slows down and is finished around 305°C. The pressure rise recorded for this setup is shown in figure 3.6. Total pressure rise is about 0.1 bar, which is 40 times less than for the regular side branch setup.

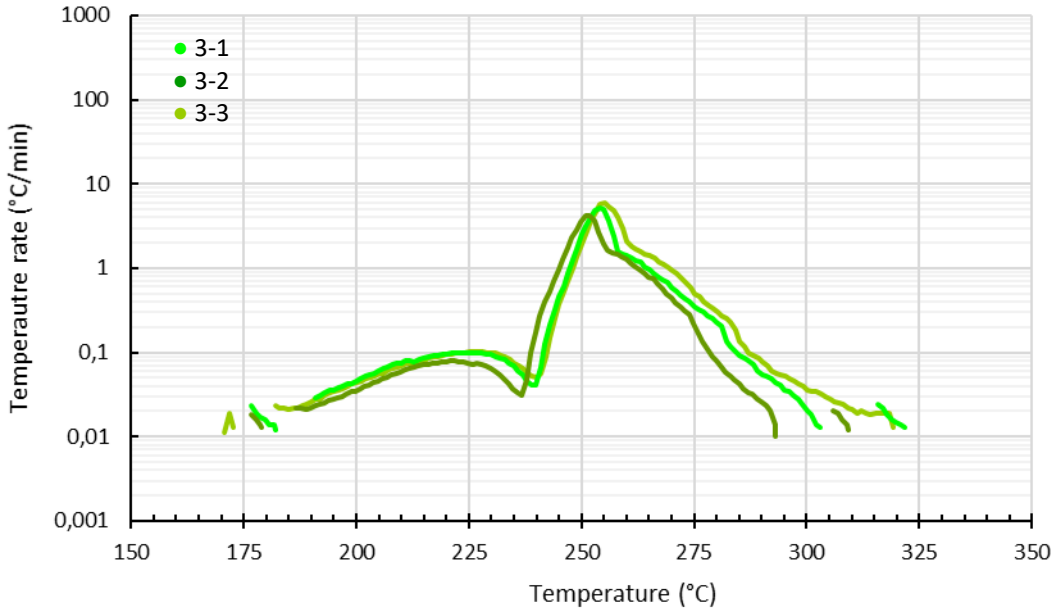

Figure 3.5 Self-heating of NMC442 with electrolyte in the large-volume side branch setup.

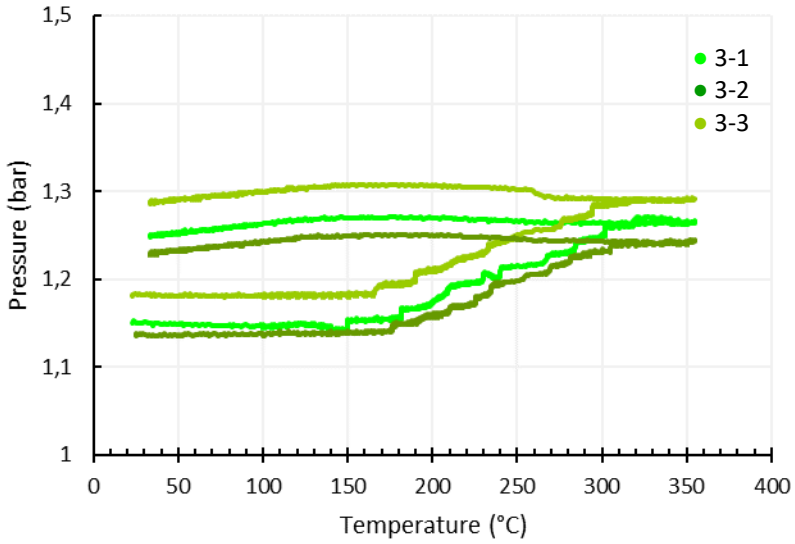

Figure 3.6 Pressure recordings for the large-volume side branch setup.

3.1.5 NMC442 with electrolyte – throne setup

The test in the throne was run to see if the connection of the sample to the calorimeter lid would have any effect on the results. The tubes in this setup were not completely sealed, only pressed shut manually, and it can be assumed that they were at atmospheric pressure. From figure 3.7, it is evident that these tests are not as reproducible as the previous setups. The exothermic onset temperatures are 180°C, 190°C and 195°C, giving an average value of 188°C. The onsets are more spread out and higher than the previous tests (which were all centred around 175°C). This irregularity is as expected, because reproducibility is limited by how equally the tubes can be closed manually. Similarly to the high-volume tests, the throne tests did not go to thermal runaway. They had a maximum heating rate of about 3°C min^{-1} on average. This result suggests that thermal runaway of the cathode material is dependent on pressure, and for open containers or low-pressure environments, the material may be less reactive.

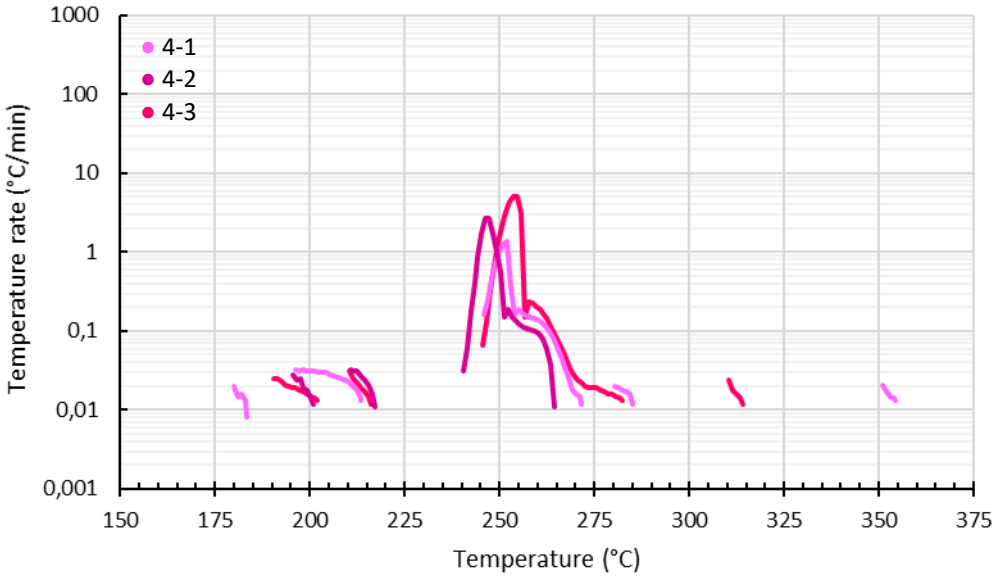

Figure 3.7 Self-heating of NMC442 with electrolyte in the throne setup.

3.1.6 Full Kokam 8Ah cell

For comparison, the full cell ARC result is shown in figure 3.8. The exothermic onset temperature is 92°C. This is where the anode SEI layer starts to decompose, leaving the anode exposed to react with the electrolyte (3, 72). After further self-heating to 130°C, the cell self-heating rate suddenly drops, as shown with the dotted line in figure 3.8. From the video recordings, ventilation was observed at this point. The cooling induced by ventilation caused the ARC to exit exotherm mode and proceed with the heat-wait-seek procedure. As the ARC was programmed to wait for 60 min, the cell continued to self-heat before exotherm mode was re-established, which is why heating recorded during wait and seek operations has been included in figure 3.8 in addition to the exotherm curve. The cell reaches thermal runaway at 209°C. The maximum temperature reached was 870°C.

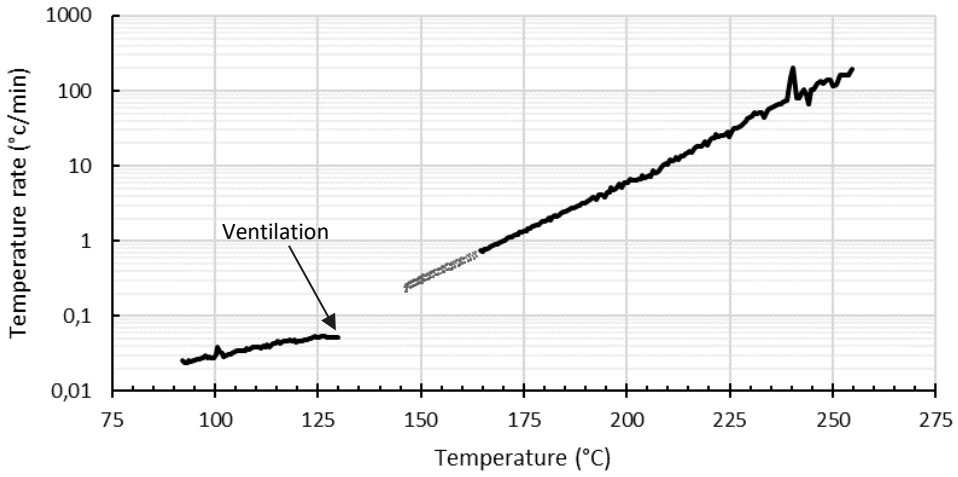

Figure 3.8 Self-heating rate vs. temperature for full Kokam 8Ah cell. The grey dotted line shows heating recorded in wait/seek mode (before exotherm mode was reinitiated), and the black solid line shows the exotherm recording.

3.2 TGA experiment: NMC442

Figure 3.9 shows the TGA/DTA plot for the cathode material. The sample experiences a 5% weight loss around 100°C, and the DTA plot shows endothermic tendencies at this temperature. The indicated endotherm could be due to evaporation of water impurities (the sample was exposed to air during loading to the TGA instrument) or solvent residues. The TGA sample was prepared with unwashed cathode material, and the electrolyte solvents of the cell are unknown. Possible solvents that could evaporate around 100°C are DMC (bp 90°C) and EMC (bp 106°C) (52). Subsequent weight loss starting slowly at 150°C, and accelerating at 250°C, could be due to phase transformation of the NMC material with O_2 release. This process is exothermic, and the DTA curve shows possible exothermic reactivity here. The DTA is not very accurate, but it may give some indications of the thermal properties of the sample.

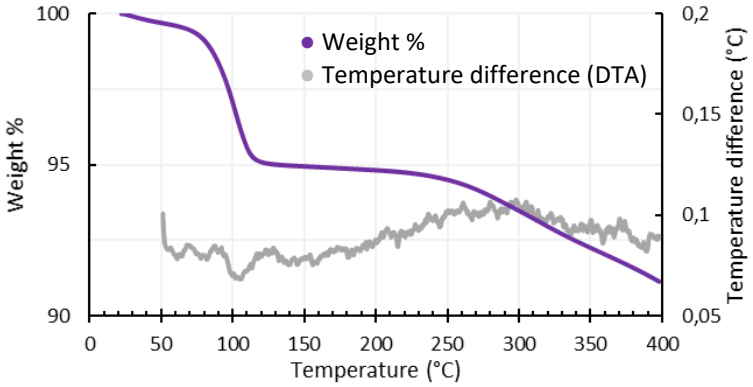

Figure 3.9 TGA and DTA plots for unwashed NMC442.

4 Discussion

The side plug setup is a standard and simple way to do the ARC experiment. It is completely pressure tight and resembles many of the setups found in literature, where the sample tubes often are welded shut, only it is connected to the calorimeter lid (23). One drawback with this setup is that it does not allow for pressure measurements. Thus, the side branch setup was also tested. Here, the sample connects to the external gas system, where it is also possible to implement gas sampling at any point during the ARC experiment. Gas sampling is one of the goals that are being worked towards with this project. To judge how the pressure influences the measurements, the expanded-volume side branch test was introduced. This setup also provides an airtight environment for near-atmospheric pressure tests. It is not known whether or not heat will escape from the sample through the lid or the external pressure system, and this would lead to lower heat measurements than the true value, which is not desired. Thus, the throne setup was included, where the sample is isolated from the ARC chamber.

Figure 4.1 shows all the material test results together for easier comparison. One of the most important observations that can be pointed out from the graphs is that the low-pressure tests (3 and 4), where the pressure was at, or close to, atmospheric pressure, do not reach thermal runaway. This clearly indicates that pressure is very important for self-heating of the cathode with electrolyte. The high-pressure tests (1 and 2) all reach thermal runaway before 260°C.

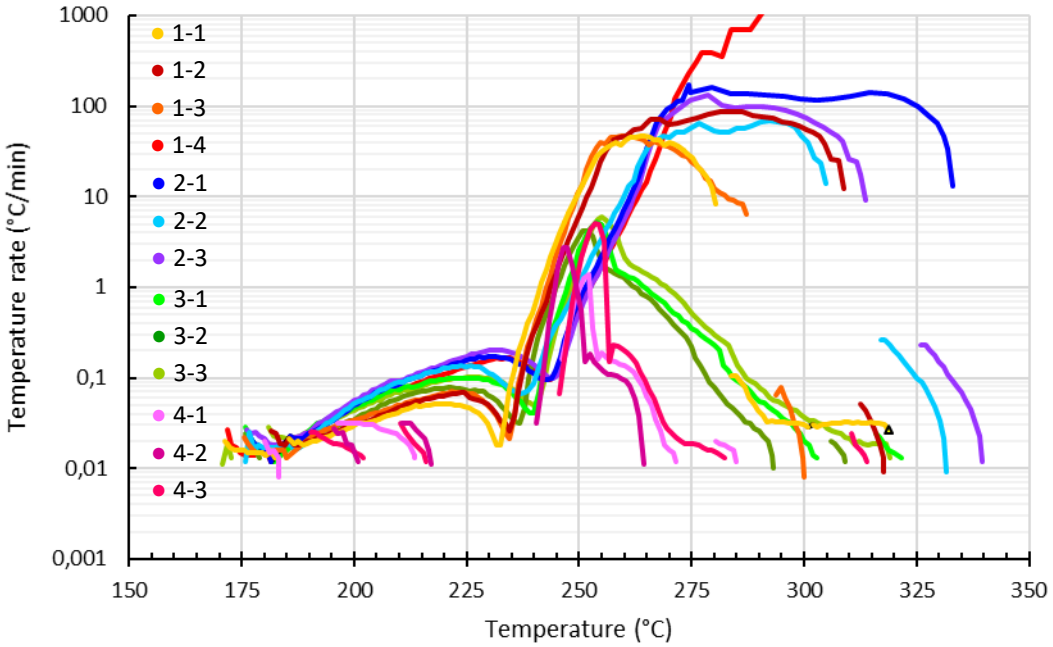

Figure 4.1 Self-heating rate vs. temperature for all NMC442 ARC tests.

Figure 4.2 shows the difference in heating rate and pressure between the side branch tests with low and high volume. From literature, the typical ARC test is run with sealed, pressure tight

sample tubes, normally without pressure measurements (35, 37, 39, 40, 61, 63, 65). This means that the results found in literature are based on high-pressure ARC tests. In real battery incidents, the cell will vent at a certain pressure, bringing the materials to atmospheric pressure. What the results in figures 4.1 and 4.2 show is that the heat generated by the cathode may not be enough to cause thermal runaway if the pressure is lowered. This is an important result, because it indicates that the current typical ARC and DSC tests may overestimate the influence of the cathode alone on thermal runaway of LIBs.

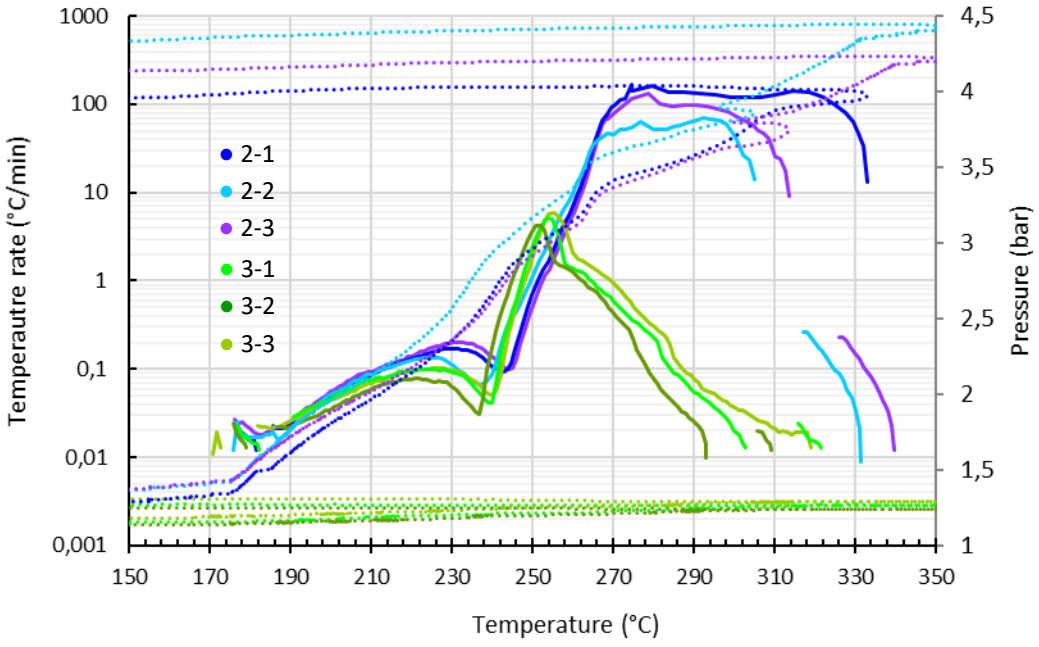

Figure 4.2 Self-heating rate (solid line) and pressure (dotted line) vs. temperature for the side branch tests with high (3) and low (2) volume.

To learn more about how ventilation affects the thermal runaway reaction, it would be interesting to do similar tests where ventilation is simulated by opening an automatic valve to the 500 mL gas bottle at a specific temperature before thermal runaway, using the side branch setup. The gas products may be analyzed by GC-MS in order to learn more about the decomposition mechanisms or identify hazardous products. Of course, gas sampling itself may alter the reactivity during thermal runaway, and the gas products detected may not necessarily be the same as for the high-pressure test. However, because venting occurs in real battery incidents, it may resemble reality more accurately than the high-pressure test. The results in this study indicate that venting at low enough pressure could slow down the self-heating of the cathode enough to prevent thermal runaway.

As seen in figure 4.1, there is some variation in the reactivity of the samples pre thermal runaway, and although it may appear as if this is due to the use of different ARC setups, the 1-4 parallel shows that it is most likely not. This test was performed 3 months after the other side plug tests, to ensure that the material had not degraded over time. Judged by the high reactivity

measured for test 1-4, there are no signs of material degradation. However, the test shows that the variation observed in the early stages of heating is not due to changes in the ARC setup. Rather, there could be a weakness in the sample preparation procedure that increases the risk of personal errors. This is supported by the fact that samples that are tested close together in time are more similar, perhaps because it is easier to do the preparations similarly when there is not a lot of time between the tests. Recalibration of the ARC before setup changes may also have contributed to variations, but the drift tests ensure that this contribution is very small. Before further discussing the procedure, it is useful to discuss the possible processes that may be occurring in the samples before thermal runaway.

All tests show an indication of two stages of heating, one in the temperature range 175-240°C, and the other starting around 240°C (see figure 4.1). In literature, the ARC results of NMC442 have a similar shape, first a slow heating followed by sinking heating rate, then a rapid increase in heating rate leading to thermal runaway (35, 37-39). It seems that the rate of the first stage influences the onset point of the second stage – higher heating rate of the first leads to higher onset temperature for the second. It is not immediately evident if the decreasing heat rate observed around 240°C is due to a break between two separate processes or an endothermic process. This part of the plots will hereby be referred to as the low point. If the plot is manipulated so that the thermal runaway reaction is aligned (figure 4.3), it is easier to see that the process looks very similar for all the setups, except the throne setup. The only difference is the heating rate and a subsequent shift in temperature of the low point.

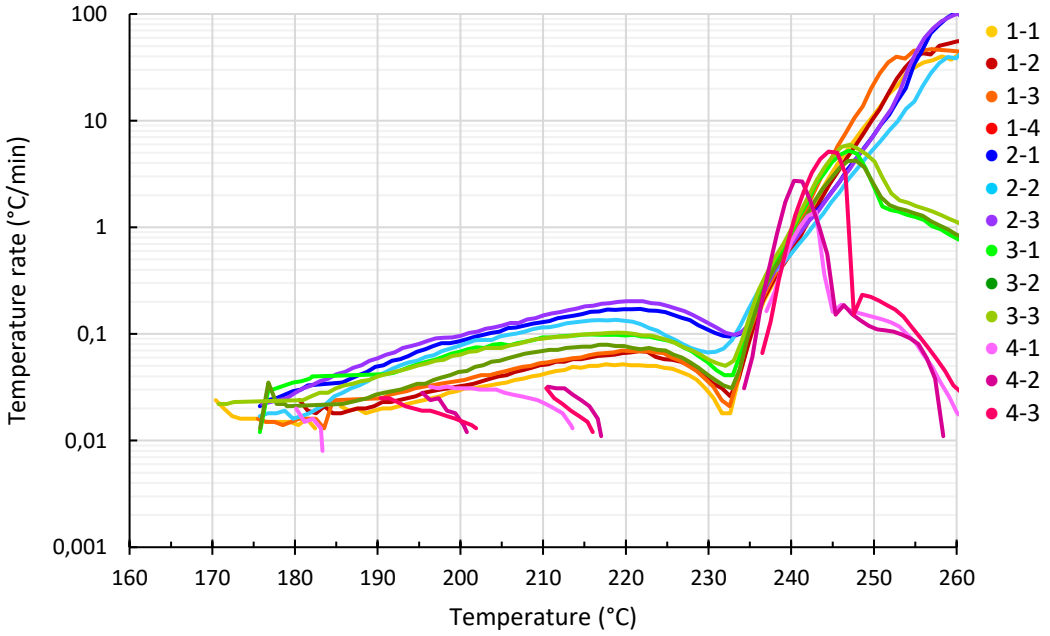

Figure 4.3 Manipulated ARC plot where the curves have been aligned.

DSC measurements of pure, delithiated NMC532 from literature show an exothermic onset temperature of around 220°C (30, 73). Bak *et al*. reported that the phase transition from layered

NMC to spinel started at 235°C for NMC532, and for NMC442 the transition is expected to occur at a slightly higher temperature (49). From this, it may look as though the sudden increase in heating rate observed after the low point in figures 4.1 and 4.3 is due to the release of O_2 accompanying the phase transition. Thus, the reactivity between 175-230°C could appear to be a different process. However, from the results of Liu *et al*., the O_2 release from NMC532 (measured by DSC-TGA-MS) very clearly starts before the recorded phase transformation (XRD) and heat evolution (DSC-TGA-MS) (30). The slow O_2 generation started at 150°C, whereas the heat generation started at 200°C. Both the O_2 release and heat generation peaks had maximum values at about 276°C. This indicates that O_2 is released from the structure before the heat released during the transition is recorded. If this starts around 150°C for NMC532, it makes sense that O_2 could be inducing early exothermic decomposition of the electrolyte, surpassing the ARC exotherm limit at around 175°C in the present experiments. The pure electrolyte solution had an exothermic onset temperature of 215°C, as seen in figure 3.1, so it is likely that the cathode somehow catalyzes the decomposition of the electrolyte. This suggestion is further supported by the TGA measurements, shown in figure 3.9, where slow weight loss is observed starting at 150°C. This should also be due to O_2 release. The TGA plot also shows accelerated weight loss around 250°C, where the thermal runaway reaction is observed in the ARC experiments. As the O_2 release before this is very small, it is possible that the DSC is not always sensitive enough to record heat generation in the early stages. It is also likely that the majority of the heat comes from reactions of the electrolyte, and not the oxygen release itself, so DSC measurements with the pure cathode material would not measure a lot of heating in this region. DSC profiles for pure NMC333 from Kim *et al*. show low heat flow starting at 160°C, accelerating at around 270°C (74). Hildebrand *et al*. reported similar results with ARC as seen in figure 4.1, and they stated that decomposition of the cathode and subsequent reaction with the electrolyte started around 160°C and accelerated around 235°C (37). If it is true that O_2 slowly starts to release at 150-175°C°C, leading to early decomposition of the electrolyte, it must be an endothermic process that is responsible for the low point before thermal runaway. In literature, a low point is usually observed for NMC442, but has not been discussed by the authors (35, 37-39). Figure 4.4 shows the ARC results with pressure measurement for one of the side branch experiments (they all had similar graphs).

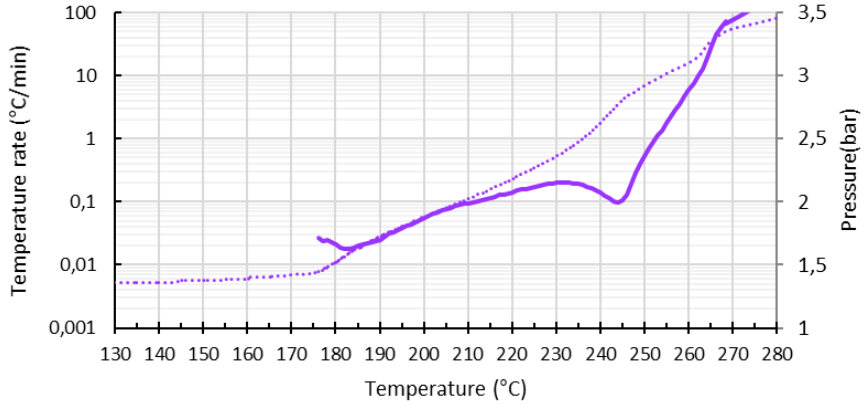

Figure 4.4 Heating rate (solid line) and pressure (dotted line) vs. temperature for ARC test 3-3.

The graph shows a small, but significant, acceleration in pressure generation where the low point in the heat rate curve is observed. This indicates that the low point could be created by an endothermic, gas-generating process that slows down the total heating rate in this region. It does not appear as if the low point is due to a break between two exothermic reactions, because that would not lead to such an increase in pressure. Additionally, there was not found any published literature stating that two distinct oxygen-releasing processes occurs for the cathode material in this temperature range.

Although they do not specifically refer to it, Liu *et al*. show an endothermic process in their DSC measurement of NMC532 with electrolyte in the supporting information (30). The low point of the endotherm is at about 240°C, just before the exotherm onset that is also observed for the pure cathode material. In addition, simultaneous TGA measurements showed weight loss during the exotherm. These results are consistent with the results shown in figure 4.4. No direct explanation of this endotherm has been found in literature. It could be evaporation of the EC solvent (bp = 244°C (52)), which would depend on pressure as well as $LiPF_6$ and DMC concentration. Thus, it is reasonable that the low-point shifts between parallels, as they show different reactivity in the early stage of heating, which does not appear to be due to differences in the setup. Evaporation is not the only endothermic, gas-generating process that could happen in this temperature range. As mentioned in section 1.4.1, some of the known electrolyte reactions are endothermic.

To understand what may be causing the small differences before thermal runaway, the sample preparation procedure should be investigated. A summary of results and sample information is listed in table-01, for reference. There was not found any correlations between reactivity and insulation amount, number of days since scraping, small difference in φ-factor or sheet number, from the limited data available from three parallels of each setup in this study. There are some possible sources of error in the sample preparation procedure that cannot be checked, and thus may be causing small variations in the results. For the tests where the sample tube is attached to the lid, there exists an uncertainty in how tightly the side branch or side tube is secured. Another problem is that the volume of the electrolyte could vary due to evaporation or small errors in pipetting during sample preparation. Additionally, the size of the cathode powder after scraping could vary, and so could the packing density inside the tube. This could lead to different electrode-electrolyte contact, which could alter the reactivity. For example, smaller or more densely packed powder particles could have better contact with the electrolyte, and it could be easier for O_2 to escape and react with the electrolyte (75). The packing of the material inside the tube could be the factor that has introduced the highest uncertainty in these experiments. In order to improve the sample preparation procedure, it could be useful to grind the material into a fine powder after scraping (40, 44). As this may be time-consuming, and also possibly change some material properties, it can at least be recommended to develop a good procedure for compression of the cathode powder inside the tube, so that this is done in the same way each time. This could be achieved by making a stamp that could compress the material to a pre-determined height inside the tube. Without such a device, it is understandable that the technique will vary over time, and tests that are run around the same time can be more similar than those that are far apart in time. Note that the temperatures sensor must not be placed above the sample

on the tube. It is unknown how small variations in the placement of the temperature sensor would affect the result.

To evaluate the sample-lid connection and its contribution to heat loss or gain, it is useful to compare the low-pressure side branch setup with the throne setup. The throne setup is designed so that the tube is isolated from the rest of the ARC chamber, so it has very low thermal mass that can absorb heat, except for the sample. The side branch test is connected to the lid. In a worst-case scenario, some of the heat generated in the sample would be transferred to the lid, which would make the recorded heating lower than the real. In figure 4.5, it can be seen that the throne tests have much lower reactivity than the low-pressure side branch tests. Thus, it can be assumed that heat loss to the lid is negligible, and the adiabatic environment is maintained for both setups. The throne setup is not air tight, so it may be that the lower reactivity is only due to this. The best way to do the throne test (as a reference test for the side plug test) would perhaps be to weld the sample tube shut instead of just closing it, but it requires additional equipment and space inside the glove box (23). Alternatively, the tube could be sealed with a Swagelok lid. This would lead to a very high φ-factor (φ = 24 as opposed to φ = 3), which may lead to the same amount of uncertainty as the open tube.

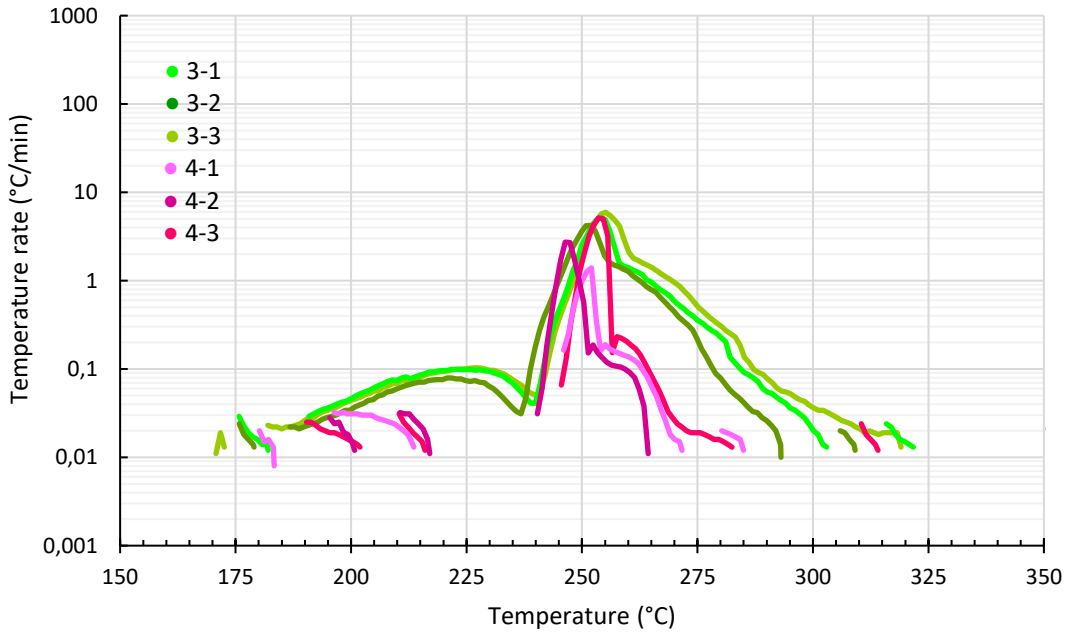

Figure 4.5 Self-heating rate for the high-volume side branch (3) and throne (4) setup ARC tests.

The self-heating of ARC samples post thermal runaway is not normally included in literature (32, 35, 37, 39, 41). In the present study, the samples that reached thermal runaway typically cooled down afterwards. This can be seen in figure 4.6, indicated with X. Gas leaks could induce this cooling effect, but the pressure measurements do not show any pressure drop at this point.

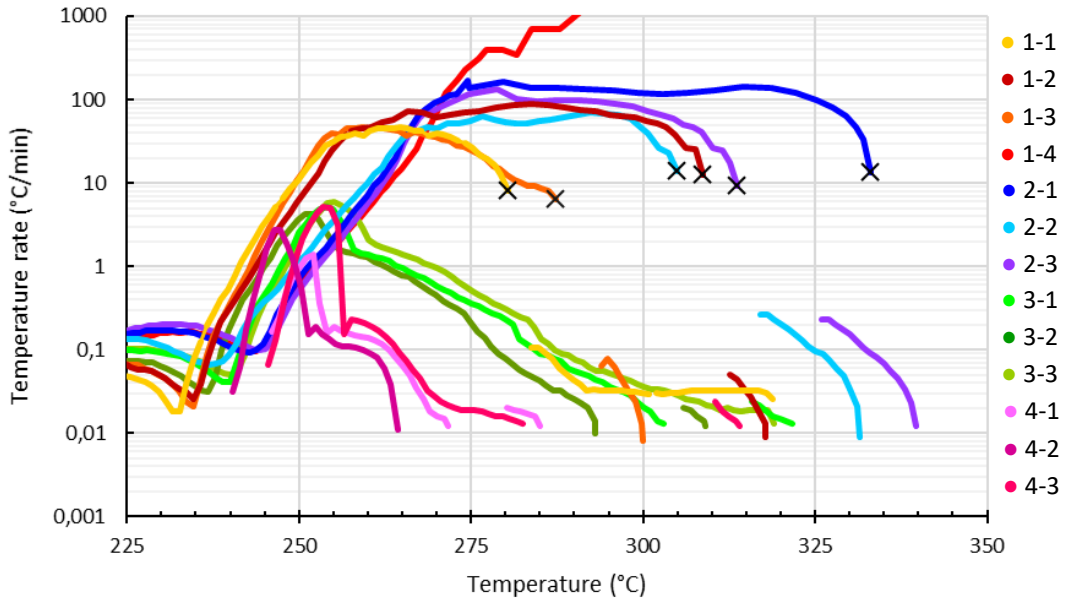

Figure 4.6 Negative heat rates after the points marked with X after thermal runaway.

Figure 4.7 shows that the cooling effect is due to a limitation of the ARC instrument. When the sample self-heating rate surpasses the ability of the ARC to match its heating, the ARC chamber is colder than the sample. When the self-heating of the sample slows down, the sample cools as a result of the colder ARC chamber before thermal equilibrium is reestablished over a few minutes. After one or two heat-wait-seek cycles, a small exotherm is usually detected by the ARC (see figure 4.5). This may be the phase transformation of NMC continuing after complete decomposition of the electrolyte, or residual electrolyte reactions.

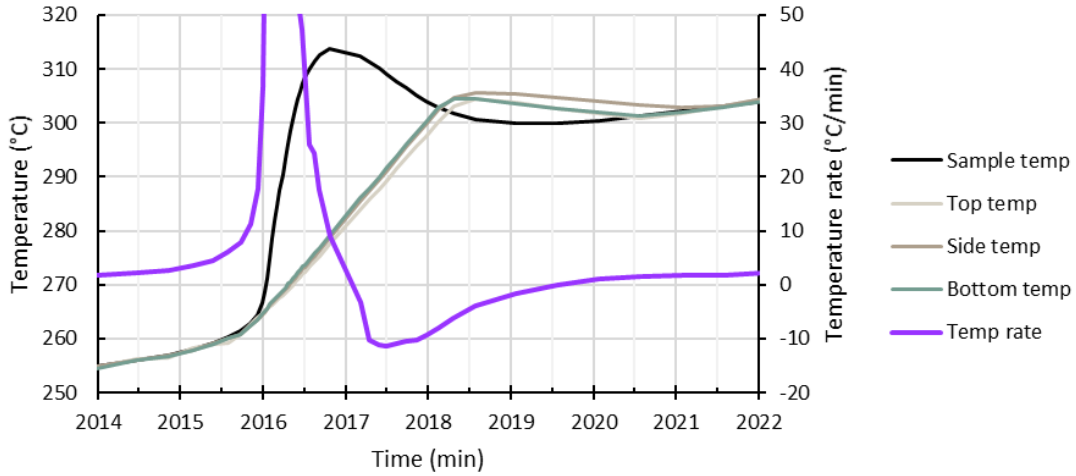

Figure 4.7 Temperature of test 2-3 vs. ARC chamber temperature (side/bottom/top) as a function of time. Sample temperature rate is also displayed.

Röder *et al*. have shown how the φ-factor of the sample can influence its recorded self-heating (36). Their results show that a lower φ-factor of 2.2 gave 10 times higher maximum heating rate than a φ-factor of 3.4 for an electrolyte sample. This underlines how important the φ-factor really is. In the present study, the φ-factor of the NMC442 tests lies around 3. It has been calculated using only the SS tube and the Al-clip, and the electrolyte has been neglected. It is not perfectly accurate because the electrolyte (and metal parts in the setup) may absorb heat. However, it has already been established that the connection to the lid does not impact the result significantly, and the most important aspect of the φ-factor in these tests is that it is comparable to the whole cell. The electrolyte content of the cell is unknown, so it has been excluded from the calculations under the assumption that the mass of the electrolyte is negligible compared to other parts of the cell. This gives a φ-factor of 2.4 for the full cell, where the anode is regarded as inactive material that only absorbs heat. For future experiments, the φ-factor of the material tests may be lowered to this level by adding more active material using a compression tool as previously suggested.

In figure 4.8, the full cell self-heating rate is compared to that of the material tests. The onset temperature for the full cell is 92°C, and the thermal runaway temperature is 210°C. The early heating of the full cell is associated with anode SEI breakdown (72).

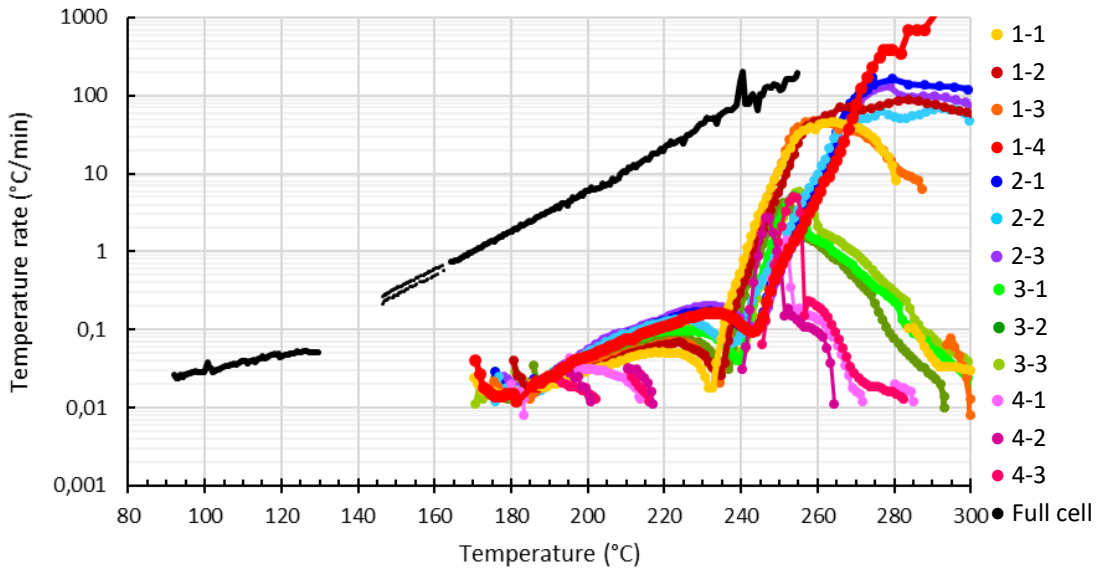

Figure 4.8 Self-heating rate of full cell compared to cathode materials.

The results in figure 4.8 are very similar to measurements by Hildebrand *et al*. on a 5 Ah pouch cell with an NMC442 cathode and a mesocarbon microbead (MCMB) anode (37). They recorded an onset temperature of about 80-90°C for the full cell, and thermal runaway was reached at around 215°C. They also did separate cathode/electrolyte tests, with an onset temperature of 165°C and thermal runaway at around 260°C. Similarly to the present experiments, their full cell tests (φ = 1.52) had a lower φ-factor than the cathode tests (φ = 1.74). It is possible that at least some of the increased recorded heating rate of the full cell above

160°C is because of a larger relative amount of thermally active material, compared to the cathode test. The self-heating of the full cell may also be intensified by chemical crosstalk between the electrodes (30). Preferably, the current measurements should have been carried out with voltage measurements, because this could identify whether a short circuit may have contributed to early heating of the full cell. It is possible that the sudden drop in pressure during cell ventilation at around 130°C may have caused the Al fixture to collapse onto the cell, pushed by the force of the springs. Investigation of the cell after the ARC test revealed an indentation in the cell where the thermocouple had been (see figure 4.9), which indicates that the thermocouple may have been pushed into the cell. This could have caused shorting of the cell. For future tests, it is recommended to remove the springs.

Figure 4.9 Photograph of the cell front post thermal runaway. The part on the left is the melted Al pouch stuck to the Pyrogel insulation material. The rest of the cell is on the right.

5 Conclusion

The importance of properly describing ARC test procedure together with results for battery material thermal stability tests was evaluated in this study, by investigating how the ARC setup could influence the results of such tests. Equal samples of $LiNi_{0.40}Mn_{0.37}Co_{0.23}O_2$ with 1 M $LiPF_6$ were placed in four different test environments. It was found that the cathode/electrolyte samples had an onset temperature for exothermic activity at 175±5°C, a possible endothermic process around 240°C and thermal runaway at 250-260°C. In setups where the pressure was close to or at atmospheric pressure, the temperature rate never reached thermal runaway, and it

was concluded that the reactivity was highly dependent on pressure. This observation underlines how important it is to consider the ARC setup when evaluating results from literature or experiments. In self-heating pre thermal runaway, the setup of the ARC test was not found to influence the result significantly. Variations in this phase of heating was attributed to lower reproducibility in the sample preparation, possibly because the material may have been packed with different density inside the sample containers. It was suggested that a stamp pushing the material down inside the tube to a certain height could be desirable for increased reproducibility. An ARC test of the full Kokam 8 Ah pouch cell gave an onset temperature of 92°C and thermal runaway at 210°C. The increased thermal reactivity of the full cell versus the cathode material was attributed to early anode reactions, followed by possible anode-cathode crosstalk and a possible short circuit. Additionally, the higher share of thermally active material in the full cell as opposed to the cathode test could have contributed to increasing the measured self-heating.

Appendix A SEM and EDS analysis of NMC442 cathode

Below are SEM images of the Kokam 8Ah cathode material. The EDS analysis is also presented. Atomic percentages: Ni: 39.6%, Mn: 36.8%, Co: 23.6%.

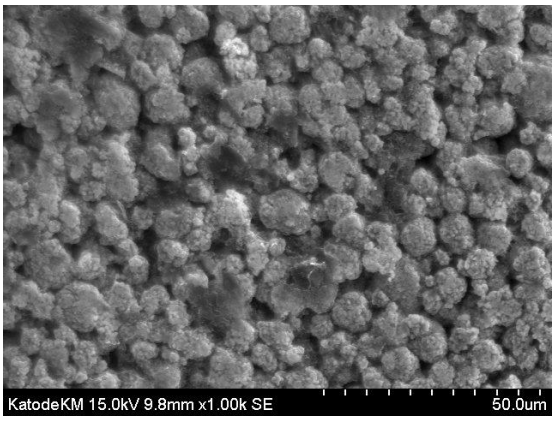

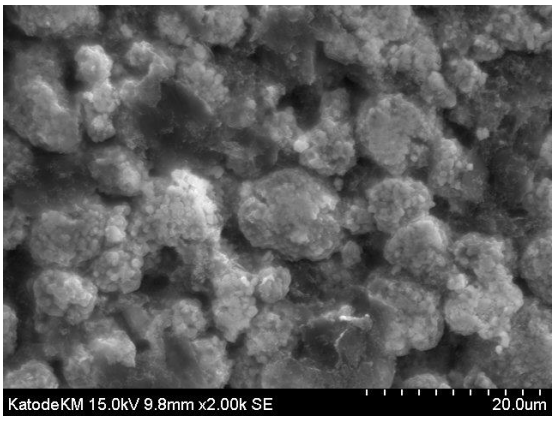

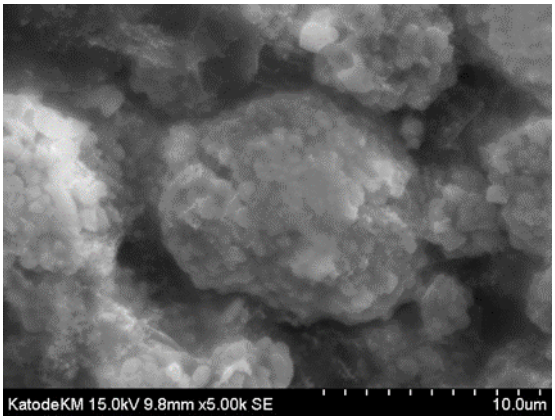

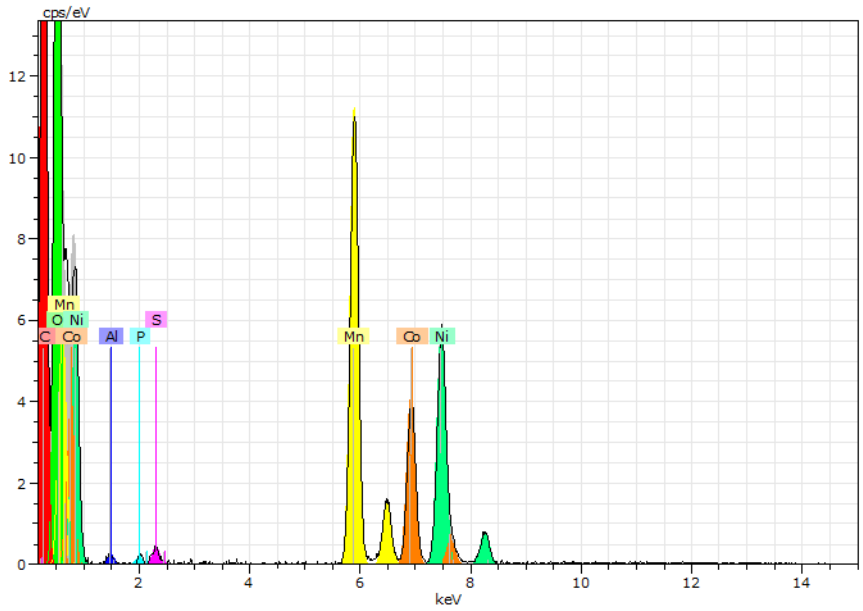

Spectrum: Kokam KM katode 12

Element	Series	unn. C [wt.%]	norm. C [wt.%]	Atom. C [at.%]	Error (3 Sigma) [wt.%]
Carbon	K-series	30,08	32,78	55,75	10,10
Oxygen	K-series	20,11	21,93	27,99	6,81
Aluminium	K-series	0,14	0,15	0,11	0,10
Phosphorus	K-series	0,08	0,08	0,06	0,09
Sulfur	K-series	0,19	0,21	0,13	0,10
Manganese	K-series	14,11	15,38	5,72	1,31
Cobalt	K-series	9,92	10,81	3,75	0,98
Nickel	K-series	17,11	18,65	6,49	1,66
	Total:	91,74	100,00	100,00	

Spectrum: Km katode Kokam 9

Element	Series	unn. C [wt.%]	norm. C [wt.%]	Atom. C [at.%]	Error (3 Sigma) [wt.%]
Manganese	K-series	27,52	35,25	36,81	2,49
Nickel	K-series	31,62	40,50	39,58	3,03
Cobalt	K-series	18,93	24,25	23,60	1,82
	Total:	78,07	100,00	100,00	

Appendix B Summary of test results and sample information

Table B.0.1 Sample information and test result summary for ARC tests.

Test	Name	Onset 1	Max rate 1	Onset TR	TR (°C)	Max rate TR	End TR (°C)	Onset 3	Sheet #	φ	Days since scrape	Insulation amount
1-3	P-1	170	0.05	232.7	249.7	46	280	284	8	3.02	14	11 mg
1-4	P-2	180	0.07	234.6	251.7	86	309	313	9	3.00	11	13
1-5	P-3	175	0.07	234.5	249.7	45	287	294	9	2.98	14	11
1 avg.		175	0.06	234	250	(59)	(292)	(297)				
2-3	B-1	175	0.17	243	261	170	333	-	10	2.98	11	16
2-4	B-2	175	0.13	239	260	67	304	317	7	2.98	15	13
2-5	B-3	175	0.19	244	262	132	313	325	7	2.98	18	24
2 avg.		175	0.16	242	260	(123)	(317)	(321)				
3-1	V-1	175	0.1	240	N/A	5	303	316	7/10	2.97	22/36	21
3-2	V-2	175	0.08	237	N/A	4.2	293	305	6	2.95	8	17
3-3	V-3	170	0.1	240	N/A	6	319	-	6	2.97	14	12
3 avg.		173	0.09	239	N/A	5	(305)	(310)				
4-1	T-1	180	0.04	246	N/A	1.4	272	281, 351	12	2.98	8	16
4-2	T-2	190	0.03	240	N/A	2.7	264	-	12	2.92	11	16
4-3	T-3	195	0.03	245	N/A	5.1	282	310	12/6/10	2.98	14	15
4 avg.		188	0.036	244	N/A	3.1						

References

1. Schipper F, Erickson EM, Erk C, Shin J, Chesneau FF, Aurbach D. Review—Recent Advances and Remaining Challenges for Lithium. J Electrochem Soc. 2017;164(1):A6220-A8.
2. Li M, Lu J, Chen Z, Amine K. 30 Years of Lithium-Ion Batteries. Advanced Materials. 2018;30(33):1800561.
3. Liu K, Liu Y, Lin D, Pei A, Cui Y. Materials for lithium-ion battery safety. Sci Adv. 2018;4.
4. Kim J, Lee H, Cha H, Yoon M, Park M, Cho J. Prospect and Reality of Ni-Rich Cathode for Commercialization. Adv Energy Mater. 2018;8.
5. Chawla N, Bharti N, Singh S. Recent Advances in Non-Flammable Electrolytes for Safer Lithium-Ion Batteries. Batteries. 2019;5.
6. Kurzweil P, Brandt K. SECONDARY BATTERIES – LITHIUM RECHARGEABLE SYSTEMS | Overview. 2009. p. 1-26.
7. Mizushima K, Jones PC, Wiseman PJ, Goodenough JB. LixCoO2 (0<x⩽1): A new cathode material for batteries of high energy density. Solid State Ionics. 1981;3-4:171-4.
8. Duan J, Tang X, Dai H, Yang Y, Wu W, Wei X, et al. Building Safe Lithium-Ion Batteries for Electric Vehicles: A Review. Electrochemical Energy Reviews. 2020;3(1):1-42.
9. Li H, Cormier M, Zhang N, Inglis J, Li J, Dahn JR. Is Cobalt Needed in Ni-Rich Positive Electrode Materials for Lithium Ion Batteries? Journal of The Electrochemical Society. 2019;166(4):A429-A39.
10. Zhang SS. A review on the separators of liquid electrolyte Li-ion batteries. Journal of Power Sources. 2007;164(1):351-64.
11. Wang Q, Jiang L, Yu Y, Sun J. Progress of enhancing the safety of lithium ion battery from the electrolyte aspect. Nano Energy. 2019;55:93-114.
12. Li Q, Chen J, Fan L, Kong X, Lu Y. Progress in electrolytes for rechargeable Li-based batteries and beyond. Green Energy & Environment. 2016;1(1):18-42.
13. Goodenough JB, Kim Y. Challenges for Rechargeable Li Batteries. Chemistry of Materials. 2010;22(3):587-603.
14. Wang A, Kadam S, Li H, Shi S, Qi Y. Review on modeling of the anode solid electrolyte interphase (SEI) for lithium-ion batteries. npj Computational Materials. 2018;4(1):15.
15. Tarascon JM, Armand M. Issues and challenges facing rechargeable lithium batteries. Nature. 2001;414:359-67.
16. Liu B, Jia Y, Yuan C, Wang L, Gao X, Yin S, et al. Safety issues and mechanisms of lithium-ion battery cell upon mechanical abusive loading: A review. Energy Storage Materials. 2020;24:85-112.
17. Ouyang D, Chen M, Huang Q, Weng J, Wang Z, Wang J. A Review on the Thermal Hazards of the Lithium-Ion Battery and the Corresponding Countermeasures. Applied Sciences. 2019;9:2483.
18. Roth EP, Orendorff CJ. How Electrolytes Influence Battery Safety. Interface magazine. 2012;21(2):45-9.
19. Zhang SS. A review on electrolyte additives for lithium-ion batteries. Journal of Power Sources. 2006;162(2):1379-94.
20. Doughty D, Roth E. A General Discussion of Li Ion Battery Safety. Electrochemical Society Interface. 2012;21:37-44.
21. Xing Y, Ma E, Tsui K-L, Pecht M. Battery Management Systems in Electric and Hybrid Vehicles. Energies. 2011;4.

22. Lu L, Han X, Li J, Hua J, Ouyang M. A review on the key issues for lithium-ion battery management in electric vehicles. J Power Sources. 2013;226:272-88.
23. Richard MN, Dahn JR. Accelerating Rate Calorimetry Study on the Thermal Stability of Lithium Intercalated Graphite in Electrolyte. J Electrochem Soc. 1999;146(6):2068-77.
24. The Accelerating Rate Calorimeter (esARC) Operations Manual. Thermal Hazard Technology. Bletchley2012.
25. Maleki H, Howard J. Role of the cathode and anode in heat generation of Li-ion cells as a function of state of charge. J Power Sources. 2004;137:117-27.
26. Höhne G, Hemminger WF, Flammersheim H-J. Differential Scanning Calorimetry. 2nd edition ed: Springer Science & Business Media; 2013.
27. Gabbot P. Principles and Applications of Thermal Analysis: John Wiley & Sons; 2008.
28. Arévalo A, Ortega G, Lozada W, Ariza I, Bautista M, Ríos J. Conceptual approach to thermal analysis and its main applications. Prospect. 2017;15(2):117-25.
29. Waldmann T, Iturrondobeitia A, Kasper M, Ghanbari N, Aguesse F, Bekaert E, et al. Review—Post-Mortem Analysis of Aged Lithium-Ion Batteries: Disassembly Methodology and Physico-Chemical Analysis Techniques. J Electrochem Soc. 2016;163(10):A2149-A64.
30. Liu X, Ren D, Hsu H, Feng X, Xu G-L, Zhuang M, et al. Thermal Runaway of Lithium-Ion Batteries without Internal Short Circuit. Joule. 2018;2(10):2047-64.
31. Maleki H, Deng G, Anani A, Howard J. Thermal Stability Studies of Li-Ion Cells and Components. J Electrochem Soc. 1999;146(9):3224-9.
32. Röder P, Baba N, Wiemhöfer HD. A detailed thermal study of a Li[Ni0.33Co0.33Mn0.33]O2/LiMn2O4-based lithium ion cell by accelerating rate and differential scanning calorimetry. J Power Sources. 2014;248:978-87.
33. Saeed R, Schlegel J, Castano Giraldo C, Sawafta R. Uncertainty of Thermal Characterization of Phase Change Material by Differential Scanning Calorimetry Analysis. International Journal of Engineering Research & Technology. 2016;5:405-12.
34. Shurtz RC, Preger Y, Torres-Castro L, Lamb J, Hewson JC, Ferreira S. Perspective—From Calorimetry Measurements to Furthering Mechanistic Understanding and Control of Thermal Abuse in Lithium-Ion Cells. Journal of The Electrochemical Society. 2019;166(12):A2498-A502.
35. Wang Y, Jiang J, Dahn JR. The reactivity of delithiated Li(Ni1/3Co1/3Mn1/3)O2, Li(Ni0.8Co0.15Al0.05)O2 or LiCoO2 with non-aqueous electrolyte. Electrochemistry Communications 2007;9:2534-40.
36. Röder P, Baba N, Fiedrich KA, Wiemhöfer HD. Impact of delithiated Li0FePO4 on the decomposition of LiPF6-based electrolyte studied by accelerating rate calorimetry. J Power Sources. 2013;236:151-7.
37. Hildebrand S, Rheinfeld A, Friesen A, Haetge J, Schappacher F, Jossen A, et al. Thermal Analysis of LiNi 0.4 Co 0.2 Mn 0.4 O 2 /Mesocarbon Microbeads Cells and Electrodes: State-of-Charge and State-of-Health Influences on Reaction Kinetics. Journal of The Electrochemical Society. 2018;165:A104-A17.
38. Jiang J, Eberman KW, Krause LJ, Dahn JR. Reactivity of Li[sub y][Ni[sub x]Co[sub 1−2x]Mn[sub x]]O[sub 2] (x=0.1, 0.2, 0.35, 0.45, and 0.5; y=0.3, 0.5) with Nonaqueous Solvents and Electrolytes Studied by ARC. Journal of The Electrochemical Society. 2005;152(3):A566.
39. Ma L, Nie M, Xia J, Dahn JR. A systematic study on the reactivity of different grades of charged Li[NixMnyCoz]O2 with electrolyte at elevated temperatures using accelerating rate calorimetry. 2016;327:145-50.

40. Cormier M, Zhang N, Liu A, Li H, Inglis J, Dahn JR. Impact of Dopants (Al, Mg, Mn, Co) on the Reactivity of LixNiO2 with the Electrolyte of Li-Ion Batteries. J Electrochem Soc. 2019;166(13):A2826-A33.
41. Huang Q, Ma L, Liu A, Ma X, Li J, Wang J, et al. The reactivity of charged positive Li1-n[NixMnyCoz]O2 electrodes with electrolyte at elevated temperatures using accelerating rate calorimetry. J Power Sources. 2018;390:78-86.
42. Jiang J, Eberman KW, Krause LJ, Dahn JR. Structure, Electrochemical Properties, and Thermal Stability Studies of Li[Ni[sub 0.2]Co[sub 0.6]Mn[sub 0.2]]O[sub 2]. Journal of The Electrochemical Society. 2005;152(9):A1874.
43. Kim G, Dahn JR. ARC Studies of the Effects of Electrolyte Additives on the Reactivity of Delithiated Li1-x[Ni1/3Mn1/3Co1/3]O2 and Li1-x[Ni0.8Co0.15Al0.05]O2 Positive Electrode Materials with Electrolyte. J Electrochem Soc. 2014;161(9):A1394-A8.
44. Ma L, Xia J, Xia X, Dahn JR. The Impact of Vinylene Carbonate, Fluoroethylene Carbonate and Vinyl Ethylene Carbonate Electrolyte Additives on Electrode/Electrolyte Reactivity Studied Using Accelerating Rate Calorimetry. J Electrochem Soc. 2014;161(10):A1495-A8
45. Röder P, Stiaszny B, Ziegler JC, Baba N, Lagaly P, Wiemhöfer H-D. The impact of calendar aging on the thermal stability of a LiMn2O4–Li(Ni1/3Mn1/3Co1/3)O2/graphite lithium-ion cell. Journal of Power Sources. 2014;268:315-25.
46. Barkholtz H, Preger Y, Ivanov S, Langendorf J, Torres-Castro L, Lamb J, et al. Multi-scale thermal stability study of commercial lithium-ion batteries as a function of chemistry and state of charge. J Power Sources. 2019;435:226777.
47. Kriston A, Adanouj I, Ruiz V, Pfrang A. Quantification and simulation of thermal decomposition reactions of Li-ion battery materials by simultaneous thermal analysis coupled with gas analysis. J Power Sources. 2019;435:226774.
48. Tsukasaki H, Fukuda W, Morimoto H, Arai T, Mori S, Hayashi A, et al. Thermal behavior and microstructures of cathodes for liquid electrolyte-based lithium batteries. Scientific Reports. 2018;8(1):15613.
49. Bak S-M, Hu E, Zhou Y, Yu X, Senanayake SD, Cho S-J, et al. Structural Changes and Thermal Stability of Charged LiNixMnyCozO2 Cathode Materials Studied by Combined In Situ Time-Resolved XRD and Mass Spectroscopy. ACS Applied Materials & Interfaces. 2014;6(24):22594-601.
50. Campion CL, Li W, Lucht BL. Thermal Decomposition of LiPF[sub 6]-Based Electrolytes for Lithium-Ion Batteries. Journal of The Electrochemical Society. 2005;152(12):A2327.
51. Gnanaraj JS, Zinigrad E, Asraf L, Gottlieb HE, Sprecher M, Aurbach D, et al. The use of accelerating rate calorimetry (ARC) for the study of the thermal reactions of Li-ion battery electrolyte solutions. Journal of Power Sources. 2003;119-121:794-8.
52. Lamb J, Orendorff CJ, Roth EP, Langendorf J. Studies on the Thermal Breakdown of Common Li-Ion Battery Electrolyte Components. J Electrochem Soc. 2015;162(10):A2131-A5.
53. Ravdel B, Abraham KM, Gitzendanner R, DiCarlo J, Lucht B, Campion C. Thermal stability of lithium-ion battery electrolytes. Journal of Power Sources. 2003;119-121:805-10.
54. Sloop SE, Kerr JB, Kinoshita K. The role of Li-ion battery electrolyte reactivity in performance decline and self-discharge. Journal of Power Sources. 2003;119-121:330-7.
55. Sloop SE, Pugh JK, Wang S, Kerr JB, Kinoshita K. Chemical Reactivity of PF[sub 5] and LiPF[sub 6] in Ethylene Carbonate/Dimethyl Carbonate Solutions. Electrochemical and Solid-State Letters. 2001;4(4):A42.

56. Yang H, Zhuang GV, Ross PN. Thermal stability of LiPF6 salt and Li-ion battery electrolytes containing LiPF6. Journal of Power Sources. 2006;161(1):573-9.
57. Solchenbach S, Metzger M, Egawa M, Beyer H, Gasteiger HA. Quantification of PF5 and POF3 from Side Reactions of LiPF6 in Li-Ion Batteries. Journal of The Electrochemical Society. 2018;165(13):A3022-A8.
58. Gnanaraj JS, Zinigrad E, Asraf L, Gottlieb HE, Sprecher M, Schmidt M, et al. A Detailed Investigation of the Thermal Reactions of LiPF[sub 6] Solution in Organic Carbonates Using ARC and DSC. Journal of The Electrochemical Society. 2003;150(11):A1533.
59. Kawamura T, Kimura A, Egashira M, Okada S, Yamaki J-I. Thermal stability of alkyl carbonate mixed-solvent electrolytes for lithium ion cells. Journal of Power Sources. 2002;104(2):260-4.
60. Andersson P, Blomqvist P, Lorén A, Larsson F. Using Fourier transform infrared spectroscopy to determine toxic gases in fires with lithium-ion batteries. Fire and Materials. 2016;40(8):999-1015.
61. MacNeil DD, Dahn JR. The Reaction of Charged Cathodes with Nonaqueous Solvents and Electrolytes. J Electrochem Soc. 2001;148(11):A1205-A10.
62. Arai H, Tsuda M, Saito K, Hayashi M, Sakurai Y. Thermal Reactions Between Delithiated Lithium Nickelate and Electrolyte Solutions. Journal of The Electrochemical Society. 2002;149:A401-A6.
63. Belharouak I, Lu W, Vissers D, Amine K. Thermal behavior of delithiated Li(Ni0.8Co0.15Al0.05)O2 and Li1.1(Ni1/3Co1/3Mn1/3)0.9O2 powders. J Power Sources. 2007;174:905-9.
64. Spotnitz R, Franklin J. Abuse behavior of high-power, lithium-ion cells. Journal of Power Sources. 2003;113(1):81-100.
65. MacNeil DD, Dahn JR. Can an Electrolyte for Lithium-Ion Batteries Be Too Stable? J Electrochem Soc. 2003;150(1):A21-A8.
66. Shurtz RC, Engerer JD, Hewson JC. Predicting High-Temperature Decomposition of Lithiated Graphite: Part I. Review of Phenomena and a Comprehensive Model. Journal of The Electrochemical Society. 2018;165(16):A3878-A90.
67. Shurtz RC, Engerer JD, Hewson JC. Predicting High-Temperature Decomposition of Lithiated Graphite: Part II. Passivation Layer Evolution and the Role of Surface Area. Journal of The Electrochemical Society. 2018;165(16):A3891-A902.
68. Haik O, Ganin S, Gershinsky G, Zinigrad E, Markovsky B, Aurbach D, et al. On the Thermal Behavior of Lithium Intercalated Graphites. Journal of The Electrochemical Society. 2011;158(8):A913.
69. Gonçalves R, Vargas J, Trevisan O. Thermal Analysis and Combustion Kinetic of Heavy Oils and Their Asphaltene and Maltene Fractions Using Accelerating Rate Calorimetry. Energy & Fuels. 2014;28:7140-8.
70. Specific heat capacity of metals Engineers Edge 2019 (Accessed July 8th 2019) [Availablefrom: https://www.engineersedge.com/materials/specific_heat_capacity_of_metals_13259.htm.
71. Specific Heats of some Metals The Engineering ToolBox 2003 (Accessed July 8th 2019) [Available from: https://www.engineeringtoolbox.com/specific-heat-metals-d_152.html.
72. Wang Q, Ping P, Zhao X, Chu G, Sun J, Chen C. Thermal runaway caused fire and explosion of lithium ion battery. Journal of Power Sources. 2012;208:210-24.
73. Wang Y, Ren D, Hsu H, Feng X, Lu L, Ouyang M. Comparison of the Thermal Reaction Kinetic Parameters of Layered Li[NixCoyMnz]O2 Cathode Material with Different Nickel Content and Different Crystal Structure. ECS Meeting Abstracts. 2019.

74. Kim H-S, Kim K, Moon S-I, Kim I-J, Gu H-B. A study on carbon-coated LiNi1/3Mn1/3Co1/3O2 cathode material for lithium secondary batteries. Journal of Solid State Electrochemistry. 2008;12(7):867-72.
75. Jung R, Metzger M, Maglia F, Stinner C, Gasteiger HA. Oxygen Release and Its Effect on the Cycling Stability of LiNixMnyCozO2(NMC) Cathode Materials for Li-Ion Batteries. Journal of The Electrochemical Society. 2017;164(7):A1361-A77.

About FFI

The Norwegian Defence Research Establishment (FFI) was founded 11th of April 1946. It is organised as an administrative agency subordinate to the Ministry of Defence.

FFI's MISSION

FFI is the prime institution responsible for defence related research in Norway. Its principal mission is to carry out research and development to meet the requirements of the Armed Forces. FFI has the role of chief adviser to the political and military leadership. In particular, the institute shall focus on aspects of the development in science and technology that can influence our security policy or defence planning.

FFI's VISION

FFI turns knowledge and ideas into an efficient defence.

FFI's CHARACTERISTICS

Creative, daring, broad-minded and responsible.

Om FFI

Forsvarets forskningsinstitutt ble etablert 11. april 1946. Instituttet er organisert som et forvaltningsorgan med særskilte fullmakter underlagt Forsvarsdepartementet.

FFIs FORMÅL

Forsvarets forskningsinstitutt er Forsvarets sentrale forskningsinstitusjon og har som formål å drive forskning og utvikling for Forsvarets behov. Videre er FFI rådgiver overfor Forsvarets strategiske ledelse. Spesielt skal instituttet følge opp trekk ved vitenskapelig og militærteknisk utvikling som kan påvirke forutsetningene for sikkerhetspolitikken eller forsvarsplanleggingen.

FFIs VISJON

FFI gjør kunnskap og ideer til et effektivt forsvar.

FFIs VERDIER

Skapende, drivende, vidsynt og ansvarlig.

FFI's organisation

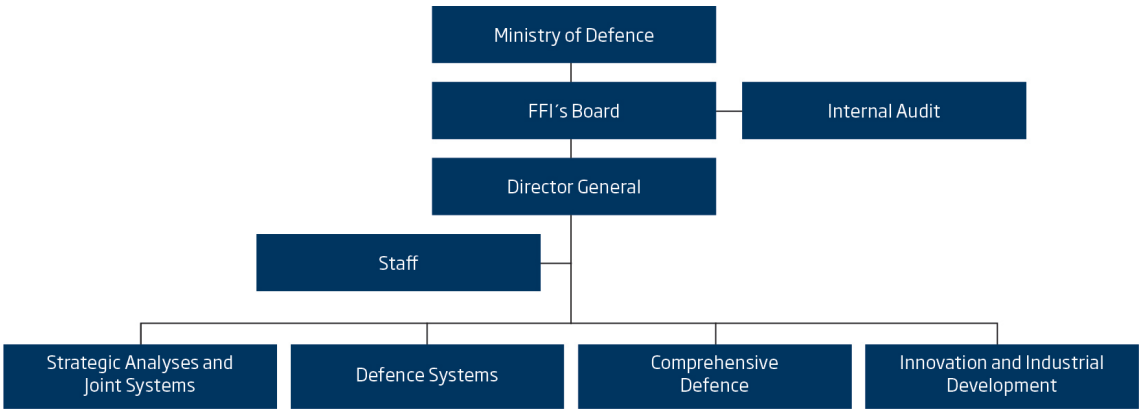

Forsvarets forskningsinstitutt
Postboks 25
2027 Kjeller

Besøksadresse:
Instituttveien 20
2007 Kjeller

Telefon: 63 80 70 00
Telefaks: 63 80 71 15
Epost: ffi@ffi.no

Norwegian Defence Research Establishment (FFI)
P.O. Box 25
NO-2027 Kjeller

Office address:
Instituttveien 20
N-2007 Kjeller

Telephone: +47 63 80 70 00
Telefax: +47 63 80 71 15
Email: ffi@ffi.no

FFI Forsvarets forskningsinstitutt
Norwegian Defence Research Establishment